Atmos. Chem. Phys. Discuss., https://doi.org/10.5194/acp-2017-1204
Manuscript under review for journal Atmos. Chem. Phys.
Discussion started: 27 April 2018

Atmospheric Chemistry and Physics Discussions

Wildfires as a source of airborne mineral dust – Revisiting a conceptual model using Large-Eddy simulations (LES)

Robert Wagner[1], Michael Jähn[1], and Kerstin Schepanski[1]

[1]Leibniz Institute for Tropospheric Research (TROPOS), 04318 Leipzig, Germany

Correspondence to: Robert Wagner (robert.wagner@tropos.de)

Abstract.

Airborne mineral dust is a key player in the Earth system and shows manifold of impacts on atmospheric properties such as the radiation budget and cloud micro-physics. Investigations of smoke plumes originating from wildfires found significant fractions of mineral dust within these plumes - raised by strong turbulent winds related to the fire. The present study revisits the conceptual model describing the emission of mineral dust particles during wildfires by pyro-convection as described by the literature. This is achieved by means of high resolved Large-Eddy simulations (LES), conducted with the All Scale Atmospheric Model (ASAM). The impact of different fire properties representing typical grassland and shrubland fires, and different ambient atmospheric conditions on the fire-driven winds and their capability to mobilize mineral dust particles were investigated. Results from this study illustrate that the energy release of the fire leads to a strong increase in strength and frequency of occurrence of intense near-surface winds, which exceed typical threshold velocities inevitably required for dust emissions. The fire-induced modulations of the wind field can be transported up to some kilometers downstream of the fire area and are able to favor dust emissions also in some distance to the fire area. Although measurements showed already the importance of wildfires on dust emissions, pyro-convection is so far neglected as a dust emission process in atmosphere-aerosol models. The results presented in this study can be seen as the first step towards a systematic parameterization representing the connection between typical fire properties and related dust emissions, which eventually can be implemented in larger-scale aerosol models ultimately contributing to the reduction of uncertainties in the aerosol-climate feedback.

1 Introduction

1.1 Occurrence and characteristics of wildfires

Biomass burning and other types of natural and prescribed wildland fires (in the following referred altogether as wildfires) are a very common phenomenon in semi-arid regions almost all over the world. In particular, tropical savannas, shrublands, grasslands, croplands, and rain forests are frequently burned ecosystems during dry seasons or under drought conditions (e.g., Gatebe et al., 2014; Roberts et al., 2009). This includes for example the Sahel zone in Northern Africa, the savannas in Southern Africa, the Amazons region, and Indonesia to name some hotspot regions. But also in other areas of the world, like North American and Siberian forests, and agricultural lands in south-eastern Europe, fires are quite often present. The burning

Atmos. Chem. Phys. Discuss., https://doi.org/10.5194/acp-2017-1204
Manuscript under review for journal Atmos. Chem. Phys.
Discussion started: 27 April 2018

Atmospheric Chemistry and Physics Discussions

regime differs significantly depending on local politics and climatic conditions as well as on the dominant land cover class, which determines the available combustion material and the dissemination of fires in general. The overwhelming majority of these fires are caused by human activity like fire clearing of natural landscapes for agriculture and domestic uses, especially popular in developing countries with a less intense agriculture. The fraction of natural fires (e.g., due to lightening) is mostly insignificant compared to the anthropogenic caused (Haywood et al., 2008).

The vulnerability of a landscape for wildfires in general and the destructiveness of fires depend strongly on the local climatic conditions and predominant weather regimes. A necessary condition for the development of a fire is the availability of a sufficient amount of biofuel (biomass). The higher the fuel load, the stronger a fire can develop. Grassland and shrubland fires are usually smaller in size and intensity compared to forest fires, whereas the typical forest vegetation provides a higher fuel load and finally a higher energy consumption by the fire occurs (Reid et al., 2005). Although a greener and denser vegetation may provide more biofuel, the higher moisture content going along with dense and green vegetation counteracts the fire risk. Compared to this, dried vegetation provides a lower fuel load, however, it is much more vulnerable for fire ignition and results into a faster fire spreading than a green and thus more humid vegetation. This leads to the strong contrast between bio-productivity building up a stock of biomass during wet seasons and the fire activity during dry seasons. For example, the North African savannas show a high fire activity during the dry season, whereas the number of fires during the wet season is usually small. Concerning the Sahel, Andela et al. (2017) suggest a decline in number and size of fires as a consequence of a transfer towards more capital-intensive agriculture and efforts to improve local air quality. In other parts of the world, an increase in fire frequency, size, and destructiveness of wildfires was observed due to increasing drought conditions, or changes in vegetation cover and land use (Chalbot et al., 2013; Keeley et al., 1999).

Wildfires have large impacts on the environment via altering atmospheric and ground properties. The heat of the fire and the corresponding fire updraft represent a major disturbance in the tropospheric wind and temperature fields, which can lead in extreme cases to a total reversal of the current weather regime culminating for example in the formation of pyro-cumulunimbus clouds from convective fire updrafts (e.g., Fromm et al., 2010). Furthermore, the fires impact strongly the surface properties in the fire-affected area. This leads to an increase in the vulnerability to wind erosion also after a fire event, since the heat of the fire removes the vegetation cover effectively and also modifies the physical and chemical soil properties like soil moisture content, mineralogy, texture, and grain size distribution (Chalbot et al., 2013; Albalasmeh et al., 2013; Merino-Martín et al., 2014). This again could result in an enhanced dust emission potential during and after a fire event, especially in already semi-arid regions.

1.2 Emission of mineral dust

The emission of mineral dust into the atmosphere is a wind-driven process and can be considered as a threshold problem (Marticorena and Bergametti, 1995). To uplift dust particles from the ground and entrain them into the atmosphere, the internal cohesive forces and binding energies between the soil particles as well as gravitation forces have to be broken by the energy supplied by the wind drag (Kok et al., 2012). The amount of energy necessary to mobilize soil particles depends on parameters such as soil moisture, soil texture, grain size, and vegetation cover (Shao, 2001). Supported by wind tunnel experiments and field measurements, typical threshold values for dust emission lie in the range between 6 and 7 $\mathrm{m\,s^{-1}}$ (Kalma et al., 1988).

Atmos. Chem. Phys. Discuss., https://doi.org/10.5194/acp-2017-1204
Manuscript under review for journal Atmos. Chem. Phys.
Discussion started: 27 April 2018

Atmospheric Chemistry and Physics Discussions

1.3 Dust emissions related to wildfires

Wildfires can effectively disturb the lower tropospheric circulation and have a strong impact on near-surface wind patterns related to a strongly increased turbulence around the fire with the formation of vertical and horizontal vortices (Clements et al., 2008). Figure 1 illustrates the conceptual model of mineral dust particle entrainment via pyro-convective updraft. The fire radiative energy released by the combustion of the vegetation heats strongly the near-surface air layers. The heated air begins to raise following the fluid dynamics of warmer air within a cooler surrounding and eventually a strong updraft forms. This upward motion results in a pressure drop of up to 1 hPa at the surface within or near the fire center (Clements et al., 2008). Subsequently, a zone of strong convergence forms and surrounding air flows towards the fire replacing the raising air. Since the ascent of the heated air above the fire area occurs quite rapid, a strong acceleration of the horizontal near-surface winds into the fire updraft region establishes, accompanied by significantly increased turbulence, enhanced vortices and possibly forming wind shear within the boundary layer (Chalbot et al., 2013; Clements et al., 2008). Together with the de-vegetation during the burning process and the accompanied dehydration of the soil surface, the resulting accelerated horizontal winds and the increased level of atmospheric turbulence are able to mobilize soil and dust particles for wind speeds exceeding the local threshold for dust mobilization. Depending on the acting buoyancy forces balancing the particles gravitation, the mobilized dust particles may reside in the atmosphere long enough to be caught up by turbulent updrafts and may mix with the combustion aerosols. Depending on the strength of the updrafts and the atmospheric background conditions, the dust particles may be injected into the free atmosphere above the planetary boundary layer (PBL). Reaching the free atmosphere, long-distance transport of the particles by the general atmospheric circulation is possible (Amiridis et al., 2010; Nisantzi et al., 2014; Ansmann et al., 2009). However, Veira et al. (2015) showed that up to 50 % of the fire plumes remain in the PBL and do not reach the free atmosphere.

The process of dust mobilization during the fire is supported by an at least partly removal of the protecting vegetation cover in the burning area. Since the fire usually moves towards the unconsumed fuel, it leaves an area of more or less bare soil behind. There, the turbulent and by the fire accelerated winds can raise efficiently soil particles due to a reduction of the local roughness length. As bare soil is more susceptible for wind erosion than vegetated soil the required threshold velocity is lower there. An additional source for dust particles emitted during wildfires are dust particles deposited on the vegetation during previous dust storms. This aspect may apply to wild fires occurring in desert margin regions like the Sahel. During combustion these particles can be mixed directly into the heated updraft and contributed to the dust load of the smoke plume (Paris et al., 2010; Cachier et al., 1995).

The strength and efficiency of dust entrainment during wildfires depend on several aspects, in which fire properties, soil conditions and state of the atmosphere are the most important. The fire properties like fire size, shape, intensity, and spreading rate determine the strength of the heated updraft and consequently the strength of convergence, the triggered turbulence around the fire, and finally the strength of the accelerated horizontal winds and its gustiness. However, the strength of the convective updraft determines also the plume injection height, which is most relevant for long-range transport of the injected particles, their atmospheric residence time, and their impacts on the atmospheric properties such as stability and dynamics, radiation budget, and cloud and precipitation forming processes.

Atmos. Chem. Phys. Discuss., https://doi.org/10.5194/acp-2017-1204
Manuscript under review for journal Atmos. Chem. Phys.
Discussion started: 27 April 2018

Several studies have proven that enhanced fractions of mineral dust particles respective enhanced concentrations of typical soil tracer species were found in numerous smoke plumes originating from different fire types such as grassland and forest fires in different areas of the world (e.g., Nisantzi et al., 2014; Kavouras et al., 2012; Diapouli et al., 2014; Maudlin et al., 2015; Alves et al., 2010; Pio et al., 2008). Nisantzi et al. (2014) used a polarization lidar located in Limassol (Cyprus) to investigate the properties of smoke plumes originating from biomass burning activity in Turkey and agriculture related fires in the region north of the Black Sea. Using the depolarization rate of the back-scattered laser light, they were able to distinguish between spherical shaped smoke particles (e.g., soot) and irregular shaped dust particles. They found dust fractions in the smoke plumes varying between 50 % for fresh plumes with an age of approximately one day and 10 % for aged plumes with an atmospheric lifetime greater than four days. The corresponding mass fraction even varies between 25 % (aged plumes) and 80 % (fresh plumes). This is mainly related to coarse-mode dust particles, which were removed during the atmospheric transport of the plume due to gravitational settlement. The dominance of coarse-mode dust particles was also found with ground-based in-situ measurements near fire locations (Gaudichet et al., 1995; Maenhaut et al., 1996). Maenhaut et al. (1996) analyzed the composition of fire-influenced particle samples in the Kruger National Park (South Africa) with "unpolluted" background samples and found a significant increase in the concentration and the mean size of typical mineral dust elements like aluminum (Al), silicon (Si), titanium (Ti), and iron (Fe) compared to the non-fire samples. The study of Gaudichet et al. (1995) points in a similar direction. By analyzing aerosol particles emitted during prescribed savanna fires in Ivory Coast, a high amount of soil particles, mostly clay and some feldspar minerals in a size range of several micrometer were found. The concentration of these soil-related minerals (Al, Ti, Fe) in fire plumes was again higher compared to background conditions with only residuals of dust particles originating from desert dust storms, suggesting that the savanna fires mobilize dust particles at the fire place or/and lead to a re-entrainment of dust particles from remote areas due to the forced upward motion above the fire area. By investigating prescribed fires in desert regions in the Western U.S., Kavouras et al. (2012) found that more than 10 % of the PM10 fire emissions can be linked to a resuspension of soil particles related to the high turbulent fire winds. Palmer (1981) already investigated the dynamics of prescribed experimental fires and highlighted the importance of the high fire-related winds in the combustion area as a source of lifted soil and dust particles. Furthermore, Radke (1991) investigated smoke plumes from prescribed and natural U.S. forest fires using airborne measurements and found particles with a size up to 1 mm and larger consisting of ash and soil remains. Despite changes in the concentration, such supergiant particles were present in all of the investigated fire sites. This underlines the importance of savanna fires as a mobilizer of dust particles, related to the high turbulence and strongly increased wind velocities in and near the fire (Susott et al., 1991). Kavouras et al. (2012) pointed that the absolute amount of dust-related emission in arid regions during fire events can be significant on a global scale, since such fires are always connected with high wind velocities and have the potential to emit mineral dust particles.

Although studies indicate the importance of such wildfires to the atmospheric dust load, the process of the dust uplift during such fire events is not well quantified so far and currently not considered as a source of airborne mineral dust in climate or aerosol models. This is all the more astonishing since the mixture of raised dust particles with fresh combustion aerosol like soot or black carbon can lead to changes in the chemical, optical, and microphysical properties of the dust particles. This has impacts on the particle formation, the dust-radiative forcing, the suitability of dust particles to act as an Ice Nuclei Particle (INP)

or as a Cloud Condensation Nuclei (CCN), which finally influence atmospheric residence time and microphysical properties of clouds and is related to health hazards (e.g., Chalbot et al., 2013; Hand et al., 2010; McCluskey et al., 2014; Levin et al., 1996; Winton et al., 2016). Such mixtures of mineral dust and biomass burning aerosol are often observed in outflows of African air masses towards the Atlantic especially in mid-tropospheric levels (e.g., Johnson et al., 2008), whereby the origin of the dust particles is not always clear and mixtures of dust and smoke can occur also during the transport (Haywood et al., 2008). Schlosser et al. (2017) investigated the aerosol composition of western U.S. wildfires plumes and found significantly enhanced levels of fine soil components and coarse mode dust particles from crustal origin within these plumes. An exemplary model simulation, done with a global aerosol model, could not capture the increased dust emission during the fires since these models were not designed to resolve the small-scale processes responsible for dust uptake in wildfires (Schlosser et al., 2017). Therefore, a better understanding of the processes is necessary to include the dust emission mechanism in aerosol models.

1.4 Usage of Large-Eddy simulations (LES) to resolve fire dynamics

Motivated by Schlosser et al. (2017), this study aims to revisit the conceptual model of mineral dust particle entrainment during fire events. To achieve this, models with a high spatial and temporal resolution are essential since the acting forces and processes leading to fire-related dust emissions occurring on very small spatial scales. A suitable and commonly used tool are Large-Eddy simulations (LES), which are able to resolve turbulent motions within the atmosphere and allow for detailed process studies without interfering influences from the surrounding like topography or large-scale synoptic systems. Therefore, LES are useful to prove hypothesis and highlight particular connections between small-scale effects.

In this context, LES are commonly used to simulate fire behaviors in different fields of application. Most of these high-resolved model studies aim to understand the spread of wildfires as a function of fuel consumption and ambient atmospheric forces to allow a better prediction of the fire spreading, primary to support the extinguishing strategies of fires (e.g., Sun et al., 2009; Mell et al., 2008; Morvan et al., 2009; Cunningham and Linn, 2007; Linn and Cunningham, 2005). In these cases a feedback of a fire and atmosphere model is necessary, which takes into account the complex interaction between the fire behavior and its environment as for example done in the WRF-Fire model (Coen et al., 2013). However, this study investigates the impacts of a fire disturbance on the near-surface wind fields and consequent potential for dust mobilization.

This paper is structured as follows: Section 2 describes the general model setup and the application to the fire simulations. Section 3 deals with the performed case studies and their representativity for real wildfires. In Section 4, the results are presented; this means in particular the impacts of the fires on the near-surface wind dynamics for different cases are shown and compared to each other. Section 5 discusses the results in a broader context with respect to the dust emission potential. The conclusion closes the paper.

2 Fire simulations with the All Scale Atmospheric Model (ASAM)

The All Scale Atmospheric Model (ASAM; Jähn et al., 2015, 2016) is a numerical solver developed at the Leibniz Institute for Tropospheric Research (TROPOS), in Leipzig, Germany. ASAM can be used for atmospheric applications over a wide range

of scales. It solves the three-dimensional, fully compressible Euler equations. Different time integration schemes are available, e.g., a split-explicit Runge-Kutta scheme (Knoth and Wensch, 2014) or an implicit Rosenbrock-type method. In the present study, ASAM is deployed as an LES model, where part of the turbulent motion is resolved directly and the remaining part is parameterized by a subgrid-scale model.

As this study focuses on the fundamental understanding of the acting processes in order to prove the basic conceptual model, the complexity of the study's design is kept low. To simulate the impacts of wildfires on the wind patterns, ASAM was set up as following: The fire itself is assumed to be stationary and represented by a constant flux of sensible heat as a measure for the fire intensity following the assumption of an ideal blackbody. This approach omits the feedback mechanism from the atmosphere acting on the fire development, which for example would drive the fire spreading and fuel consumption. The fire heat source was put at the surface layer of the model as it is typically for grassland and shrubland fires.

The horizontal extent of the model domain was set to 6.4 x 1.2 km^2. This size ensures that the fire-induced atmospheric dynamics can develop undisturbed within the model domain and are not influenced by boundary effects. The longer extent in x-direction is aligned with the flow direction. The atmospheric flow was initialized in x-direction (u-component of the wind) only, whereas in y-direction only turbulent fluctuations of the wind occur. A schematic plot of the x-y-plane of the model domain is given in Fig. 2. The fire area is located 100 m away from the inflow boundary and centered in y-direction. Using periodic boundary conditions, valuable for the formation of a turbulent PBL, the position of the fire area would be in principle arbitrary. The top of the model domain is set to 4,000 m with a damping layer at the upper 200 m, which allows for an undisturbed spreading of the fire-related updraft. The horizontal grid spacing was set to 10 m, the vertical grid spacing was set to 10 m for 0 to 1,000 m altitude, set to 20 m for 1,000 to 2,000 km altitude, and set to 40 m for altitudes above 2,000 km. Using an explicit Runge-Kutta scheme, the initial model time step was set to 0.2 s.

To investigate the impacts of the fire on the near-surface winds as realistic as possible, the fire was ignited already in a turbulent PBL as suggested by the model study of Sun et al. (2009), who found that the usage of a time-averaged wind within the PBL does not map the fire properties and the interaction with the atmosphere in such a correct way, as a more realistic turbulent PBL does. The formation of such a turbulent PBL requires a spin-up time of the model while the turbulent nature of the PBL can develop. After forcing initial perturbation of the temperature field of 0.2 K, two hours later it can be guaranteed that a widely stable and representative PBL with a largely constant depth has developed, so that the fire can be initialized. Due to the periodic boundary conditions, the simulations were stopped at the time when the fire-influenced atmospheric field transported downstream by the ambient air flow reaches the end of the model domain or at latest 40 min after fire ignition. Thus, in total each simulation covers at maximum 2 h 40 min.

Since the fire occurrence peaks in semi-arid regions, a typical dry-season atmospheric profile over the Sahel, one of the global fire hotspots, was representatively used. This profile was compiled using model outputs of the meso-scale model COSMO-MUSCAT (Tegen et al., 2013; Wagner et al., 2016) by averaging the wintertime atmospheric fields 2007/08 of the Sahel region.

Atmos. Chem. Phys. Discuss., https://doi.org/10.5194/acp-2017-1204
Manuscript under review for journal Atmos. Chem. Phys.
Discussion started: 27 April 2018

3 Sensitivity studies of different controlling factors

To prove the conceptual model of dust emission related to wildfires in general and to investigate the influence of possible fire-related controlling factors, sensitivity studies with different input parameters were conducted. The main focus lies on the variation of the fire properties and the ambient wind velocity as the probably most important factors influencing the fire-related wind pattern. Additionally, a non-fire simulation (case 0) with an undisturbed non-fire PBL was performed as a reference. An overview of all performed case studies is given in Table 1. If not affected by the chosen setup (see Table 1), the following parameters were kept constant for all other case simulations:

(1) roughness length: z_0 = 0.1 m
(2) ambient wind velocity: $|u_{10\mathrm{m}}| = 3\,\mathrm{m\,s^{-1}}$
(3) fire sensible heat flux: $F_{\mathrm{fire}} = 150\,\mathrm{kW\,m^{-2}}$
(4) fire size: A_{fire} = 70 x 100 $\mathrm{m^2}$ = 7,000 $\mathrm{m^2}$
(5) fire shape: rectangular

The roughness length was set to 0.1 m as a typical mean value for grassland and shrubland dominated landscapes, the primarily burned vegetation classes (Roberts et al., 2009; Gatebe et al., 2014). The average wind velocity of $u_{10\mathrm{m}} = 3\,\mathrm{m\,s^{-1}}$ was chosen, since this value represents a well-balanced equivalent to typical atmospheric conditions and within a range often reported as background wind conditions during wildfires (e.g., Coen et al., 2004; Clements et al., 2007; Clark et al., 1999; Frankman et al., 2013; Lareau and Clements, 2017). To cover a broader range and investigate the impacts of different wind velocities on fire-related dust emission potential also weaker ($u_{10\mathrm{m}} = 1\,\mathrm{m\,s^{-1}}$, case 1) and stronger ($u_{10\mathrm{m}} = 5\,\mathrm{m\,s^{-1}}$, case 3) ambient wind conditions were simulated. The ambient wind was forced with a logarithmic wind profile only in x-direction, so that due to the turbulent nature of the simulated PBL, the values of the ambient wind velocity represent the mean wind velocities in x-direction before fire ignition. The average wind speed in y-direction is around zero due to a compensation of positive (northern) and negative (southern) fluctuations.

In order to investigate the influence of different fire properties on the fire-related wind fields as broadly as possible, the fire intensity, size, and shape were modified. One of the main fire quantities is the fire intensity, expressed by a flux of sensible heat released by the fuel consumption. Values reported in the literature vary quite substantially in orders of magnitude depending the fuel type, the atmospheric conditions, fire behaviors as well as the measuring procedure and are in a range of $8\,\mathrm{kW\,m^{-2}}$ to $3\,\mathrm{MW\,m^{-2}}$ (Lareau and Clements, 2017), whereby the intensity is usually increasing from small grassland fires to stronger forest (crown) fires (Frankman et al., 2013). Peak fluctuations of the heat flux can reach in heavy crown fires values of up to $11\,\mathrm{MW\,m^{-2}}$ (Coen et al., 2004). In general, the heat fluxes within one fire can fluctuate strongly, making it difficult to link one fire type with an exact corresponding heat flux. But nevertheless some representative scenarios can be applied. Since the focus of this study lies on grassland and shrubland fires, corresponding to the fire types heat fluxes of $75\,\mathrm{kW\,m^{-2}}$ (case 4), $150\,\mathrm{kW\,m^{-2}}$ (standard value, case 2), and $270\,\mathrm{kW\,m^{-2}}$ (case 5) were chosen. These heat fluxes represent typical values for a

Atmos. Chem. Phys. Discuss., https://doi.org/10.5194/acp-2017-1204
Manuscript under review for journal Atmos. Chem. Phys.
Discussion started: 27 April 2018

Atmospheric Chemistry and Physics Discussions

weaker grassland fire, moderate and more intense shrubland fires (Frankman et al., 2013; Clements et al., 2007; Lareau and Clements, 2017). The corresponding fire radiative temperatures (assuming a perfect blackbody with an emissivity of 1) are approximately 800, 1,000 or 1,200 °C, respectively. Since the fire is only represented by a heat flux from the surface, the fire temperatures are not directly reflected in the same order of magnitude in the near-surface air temperature fields.

The fire size does not correspond directly to any physical determined fire properties and can vary by orders of magnitude from case to case. Therefore, the values here are more or less randomly set and will only represent the impacts of differently large fire areas. Originating from the standard fire size of 7,000 m^2 (case 2), a smaller (40x60 = 1,800 m^2, case 6) and a larger (90x130 = 11,700 m^2, case 7) fire area were simulated.

Additionally, the fire shape was investigated using two line fires of the same size but with a length of 350 m and a width of only 20 m. Their only difference is the orientation of the line with respect to the mean flow direction; one fire is orientated perpendicular (case 8), the other one parallel to the wind direction (case 9). The line fire setup was chosen since prescribed grassland fires are often ignited in a line and such fires will most probably interact in a different way with the atmospheric dynamics. Thus, in total 9 different model setups were investigated.

4 Results – impacts of fires on the wind fields

In the following section the impacts of the fires on the near-surface wind pattern will be analyzed and the importance on the dust emission potential will be characterized. First, a representative overview of the fire-influenced near-surface wind pattern around the fire center is given for all case simulations 20 minutes after fire ignition. Therefore, Fig. 3 presents horizontal cross sections of the *x*-*y*-plane for the lowest model level (z = 5 m) and vertical cross sections of the *x*-*z*-plane through the center of the fire (y = 600 m) are presented in Fig. 4. Beside the wind vectors also the air temperature fields are shown in order to indicate the position of the simulated fire and the fire updraft region. Focusing on the horizontal cross sections (Fig. 3), the fire areas are clearly visible as zones of strongly enhanced temperatures, a consequence of the intense flux of sensible heat warming the near-surface air layers. Here, 5 m above ground level, air temperatures are increased by up to more than 150 K compared to the ambient conditions, where only small temperature fluctuations of up to 1 K occur as a consequence of the turbulent nature of the PBL. Variations in the size and extent of the fire areas between the different simulation setups become obvious. They are related to differences in the original fire size (Fig. 3f, g) and shape (Fig. 3h, i) but also due to impacts of the ambient wind velocity (Fig. 3a-c). Whereas in case of calm ambient conditions (Fig. 3a, case 1) the original rectangular fire shape remains more or less unchanged, a strong deformation with a bulge in flow direction occurs under higher ambient wind conditions (Fig. 3c, case 3). Regarding the horizontal wind fields, in average a west wind (eastward wind flow) is present, resulting from the inflow wind velocity forced in *x*-direction. Additionally, some areas of convergence and divergence, increased and decreased velocities resulting in small turbulent eddies are present. Zones of strong convergence along with an acceleration of the horizontal winds can be found at and in front of the leading fire edges for the majority of the case simulations (Fig. 3). These regions of convergence developed due to the intense updrafts over the heated fire areas, consistent with the findings of Sun et al. (2009). The corresponding upward motions are clearly visible in vertical cross sections (Fig. 4),

where the initial west-east-flows with only small disturbances are interrupted by upward oriented wind vectors within a defined band of increased temperatures. The areas of strongly increased upward motion are not continuously and in higher altitudes mostly not located directly above the fire area. This behavior is caused by the influence of the ambient flow, which leads to a downstream transport of the updraft and causes strong turbulence around the area of the heated air. This turbulence generates large eddies, which result in a strong relocation of the atmospheric pattern around the fire updraft. Although the figures show only snapshots of the highly turbulent nature of the fire-driven wind fields, some differences concerning the orientation and strength of the fire updrafts can be derived. In case of weak ambient wind velocities (Fig. 4a, case 1), the updraft has a defined vertical orientation with only small impacts on the remaining atmosphere. In contrast to that, under much stronger averaged ambient wind conditions of for example 5 m s^{-1} (Fig. 4c, case 3), the heated air is predominately transported in flow direction and does not reach an altitude larger than 600 m above ground level within the first kilometer downstream the fire. Hence, calm ambient wind conditions lead to an intense upward motion of the heated air, stronger winds tend to a more horizontal plume orientation. All other cases show a more or less similar plume orientation due to the similar ambient wind velocity (3 m s^{-1}). Major differences between the remaining simulations (case 4-9) affect mainly the strength of the winds originating from the fire area. As expected, they are very pronounced during stronger (Fig. 4e, case 5) and larger (Fig. 4g, case 7) fires, which provide a higher energy release, and comparably weak for the weaker (Fig. 4d, case 4) and smaller (Fig. 4f, case 6) fires. Also the line fires, especially the perpendicular orientated one (Fig. 4h, case 8), generate weaker updrafts.

The increased atmospheric turbulence triggered by the fire updraft can be expressed by the turbulent kinetic energy (TKE) as shown in Fig. 5 for all simulations including the non-fire simulation (case 0), again 20 min after fire ignition. The TKE is a measure for the turbulence of a wind field compared to a laminar, undisturbed flow. Regarding the non-fire situation (Fig. 5a, case 0), a well mixed turbulent PBL developed with a vertical extent of roughly 900 m. Here, the typical structure of the PBL is dominated by some defined vortices. Above the PBL, a largely undisturbed free atmosphere is present with very low TKE values. Differing from that, the TKE in all other simulations is strongly enhanced by up to a factor of 50 within the fire-influenced atmosphere, whose horizontal extent varies from 1,000 to 3,000 m downstream of the fire area depending on the chosen setup. For all simulations the zone of substantially increased turbulence exceeds the modeled PBL and interacts with the free troposphere. Due to the forcing of the ambient wind flow, the enhanced turbulence is transported downstream and weakens only slowly with growing distance to the fire area. This downwind transport of TKE results in an increased level of turbulence which also affects areas in some distance to the fire. There, the development of wind gusts can be favored due to downward mixing of momentum and a modification of the "normal" non-fire atmospheric wind conditions occur. Comparing the individual simulations, differences in strength and extent of the fire influenced pattern become obvious. The penetration depth of the fire updraft into the free troposphere differs quite substantially and is strongest under weak ambient wind conditions (Fig. 5b, case 1) but also above average in case of larger and more intense fires (Fig. 5f and g, case 5 & 7). The impacts of weaker and smaller fires (Fig. 5e and f, case 4 & 6) are more limited to the simulated PBL but here as well connected with a strong disturbance of the atmospheric layering. The downstream horizontal extent of the fire related turbulence is driven by the strength of the ambient wind velocity but surprisingly the fire shape seems important as well. The perpendicular oriented line

Atmos. Chem. Phys. Discuss., https://doi.org/10.5194/acp-2017-1204
Manuscript under review for journal Atmos. Chem. Phys.
Discussion started: 27 April 2018

fire (Fig. 5j, case 8) leads to a strongly increased near-surface turbulence also some kilometers downstream of the fire area, while areas of increased TKE are much more lifted in the other setups.

Differences in the updraft orientation with respect to the ambient wind and the fields of the TKE can also be expressed by vertical profiles of the horizontal and vertical peak wind velocity (case 1-3) as depicted in Fig. 6. Here, vertical profiles are shown with respect to the distance to the fire. In order to further elaborate the impact of the fire on the wind fields at different distances to the fire, three zones (boxes A, B, and C) located at different distances to the fire area are defined as illustrated in Fig. 2. Each box has a size of 84,000 m^2. Box A covers the fire area itself with an extent of 240x350 m^2, Box B is shifted slightly downstream to $x = 400$ m and has an extent of 120x700 m^2, whereas Box C is located 1,000 m remote from the fire area at x=1,200 m and covers an area of 70x1,200 m^2.

Figure 6 demonstrates the vertical profiles of maximum wind velocities for the three boxes representing areas of different distance to the fire and thus the source of atmospheric disturbances. Although maximum values are given, these values still represent an average of the highest wind speeds that occur at every time step once the box-area is affected by the fire. This approach is chosen in order to avoid a vanishing of the particular high fire-affected wind velocities due to a merge with the uninfluenced wind field around the fire updraft or corresponding downdrafts. Figures 6a and 6d show the vertical profiles of both wind components (horizontal and vertical wind) directly around and above the fire center (box A in Fig. 6), Figs. 6b and 6e do the same for the area a bit downstream of the fire region (box B) and Figs. 6c and 6f illustrate the situation further away from the fire (box C). Compared are the profiles of the undisturbed non-fire PBL (dashed lines) with the profiles after fire ignition (solid lines) for the scenarios with a different ambient wind velocity (case 1-3).

First, with regard to the undisturbed non-fire wind profiles (dashed lines), the height of the modeled PBL of roughly 900 m is quite visible. Above this altitude, the horizontal wind peaks are close to the average ambient wind velocity and the vertical wind velocity close to zero, representing together a widely undisturbed, laminar flow. After fire ignition, drastic changes develop in all scenarios but show large differences between the cases and with respect to the fire distance. By comparing the profiles with increasing distance to the fire area (box A-C) a weakening and a lifting of the regions with the highest values happen. While close to the fire region the strongest impacts occur in the near-surface levels (up to 100-200 m), the influences near the surface are largely insignificant for distances > 1,000 m but higher atmospheric levels become much more influenced by downstream and upward transport of the fire-related turbulence, also above the PBL.

The patterns of the fire impact on the horizontal and vertical wind maximums depend considerably on the ambient wind velocity. During calm conditions (case 1), the fire energy is mainly transformed into an upward motion, which means a strong modification of the atmospheric circulation up to a height of around 2,000 m above ground level. Due to the strong turbulence occurring around the fire updraft also the horizontal winds are affected, leading to enhanced horizontal wind peaks, whereas in case of higher ambient wind velocities the conditions in these levels quickly turn to the normal non-fire behavior. In contrast to the weak ambient wind scenario, in presence of higher ambient wind forces (case 2 and 3) the updraft strength is much weaker but modulations in the near-surface horizontal winds are stronger. Due to the faster downstream transport of the fire-generated turbulence, the vertical extent of the fire impacts is smaller but horizontally longer present.

Atmos. Chem. Phys. Discuss., https://doi.org/10.5194/acp-2017-1204
Manuscript under review for journal Atmos. Chem. Phys.
Discussion started: 27 April 2018

The fire properties modulate the scenario in the expected way that a larger and stronger fire and the perpendicular orientated line fire lead generally to higher horizontal and vertical peak wind velocities, and impact also higher altitudes of the atmosphere. But they are, concerning the general behavior, widely comparable to the case 2-scenario, which suggests that the ambient wind velocity is the main driver of the different spreading of fire-induced winds within the atmosphere.

The quantity of the change of the atmospheric wind pattern apart from the direct surface-near levels is particular important for the distribution and further transport of once emitted particles. Especially in the presence of a non-negligible ambient wind, the occurring downstream and vertical transport of the fire-induced turbulence can still affect the atmospheric layering in some distance to the fire and can lead to an exchange between the PBL and the free troposphere, which may be important for the transport of particles, injected first only into the PBL before such processes may allow a further atmospheric distribution.

As diverse as the fire updrafts have developed, the strength of the horizontal convergence near the surface differs (Fig. 3). Comparably to the updraft strength the convergence is particular heavy during the more intense (Fig. 3e, case 5) and the larger (Fig. 3g, case 7) fires. In the presence of higher ambient winds, the convergence zone is shifted further downstream (Fig. 3c, case 3), while during calm conditions the convergence takes place right within the fire area and leads partly to a reversal of the flow direction (Fig. 3a, case 1) back to the fire area.

Since the focus of this study lies predominately on the potential of wildfires to mobilize soil dust particles and the emission of mineral dust is a threshold phenomenon, the crucial point is the occurrence of high wind speeds at the surface. To investigate the frequency of occurrence and the strength of such strong winds or gusts, Probability Density Functions (PDFs) of the horizontal wind velocity 5 m above ground were calculated. In order to analyze the impacts of the fire, the fire-affected wind PDFs are compared to the PDFs of the undisturbed non-fire winds. The non-fire wind PDFs are calculated from the last 5 minutes before fire ignition, when the PBL is fully developed. Accordingly, the calculation of the PDFs representing the fire-induced wind fields with respect to different distances to the fire area (boxes A-C) uses all time steps directly after fire ignition (box A) or even later after it can be guaranteed that the downstream transported fire-induced wind patterns reach the area of interest, which means 10 min after fire ignition for box B and further 10 min later for box C. In Figure 7, PDFs of the horizontal near-surface wind velocity in the fire surrounding (box A in Fig. 2) are shown for all case studies. The PDFs are sorted following their impacts of ambient wind velocities (Fig. 7a), fire intensities (Fig. 7b), fire sizes (Fig. 7c), and the fire shape (Fig. 7d). Additionally, fractions of wind velocities exceeding a non-fire limit of usually $6\,\mathrm{m\,s^{-1}}$ (except for case 1 and 3) are given in Table 2 for different distances to the fire area (boxes A-C, cf. Fig. 2).

The non-fire wind speed distribution as illustrated by dashed lines in Fig. 7 follows a gaussian distribution with the most frequently occurring wind velocities in the order of magnitude of the initial ambient wind velocity ($3\,\mathrm{m\,s^{-1}}$), except for cases 1 and 3, for which the mean wind speeds are 1 and $5\,\mathrm{m\,s^{-1}}$. These wind velocities fluctuate up to $3\,\mathrm{m\,s^{-1}}$ around the average due to the turbulent nature of the modeled PBL. During the presence of a fire, the whole distributions are shifted towards higher values with a significant increase of high wind velocities, which were not present before fire ignition in the non-fire PBL (cf. Table 2).

Figure 7a contrasts the fire-influenced wind PDFs for scenarios with different ambient wind velocities. It stands out that by $2\,\mathrm{m\,s^{-1}}$ increased mean wind velocity between the individual scenarios leads to a nearly perfect shift of the undisturbed

Atmos. Chem. Phys. Discuss., https://doi.org/10.5194/acp-2017-1204
Manuscript under review for journal Atmos. Chem. Phys.
Discussion started: 27 April 2018

Atmospheric Chemistry and Physics Discussions

non-fire wind PDFs towards 2 m s^{-1} higher wind velocities. Also the upper end of the distribution, the peak wind velocities, shows largely an increase by 2 m s^{-1} for each case.

The fire-influenced PDFs behave differently. A shift of the distribution towards higher wind velocities is always present, in which this shift is smallest for the low ambient wind scenario (case 1) compared to the other setups (cases 2 and 3), for which the whole distribution is shifted by roughly 1 m s^{-1}. The maximum occurring wind velocities diverge from this picture, although the development of strongly enhanced wind gusts is indeed present for all scenarios. A higher ambient wind is connected to a much more frequent occurrence of wind velocities above the non-fire limit (cf. Table 2). Under weak ambient wind conditions (case 1) only 7.4 % of the resulting winds around the fire area (box A) exceed the non-fire limit, while this value is nearly twice as high in presence of a higher ambient wind. However, the in total highest occurring wind speeds (cf. Table 3) are much closer together. In case of a weak ambient wind, the peak velocity is with 9.9 m s^{-1} even slightly greater than in case of the setup with a by 2 m s^{-1} higher ambient wind (case 2) for which only a peak velocity of 9.3 m s^{-1} occurs. Also, the peak wind velocity of case 3 is with 10.6 m s^{-1} only minimal higher. However, the frequency of occurrence of such intense wind gusts is very small in case 1 compared to the other scenarios. This particular behavior is a consequence of the calm surrounding conditions, which support the evolution of heavier accelerated surface winds because the heated air is strongly orientated upward and horizontal turbulence is suppressed. In contrast, higher ambient wind velocities lead to a more intense turbulence caused by the more horizontally orientated plume and downward mixing of momentum. The increased turbulence can disturb the evolution of very strong wind peaks but also leads to an in total much more frequent occurrence of higher wind gusts near the surface.

Figure 7b compares the change of the wind speed distribution related to different fire intensities. In all cases, a distinct and quite similar shift of the whole fire-affected PDFs towards higher velocities occurs, in total only slightly stronger for more intense fires like case 5. Generally, the maximum wind speeds reveal a clear connection between the fire intensity and the fraction of such wind velocities. More intense fires have a more frequent occurrence of strong above-average wind velocities (up to 20 % in our strongest setup compared to 6 % in the weaker fire simulation) and are in general connected to stronger accelerations of the horizontal near-surface winds.

The dependency of the wind speed distribution on the fire size as shown in Fig. 7c for the rectangular fires with a size of 1,800, 7,000, and 11,700 m^2 (case 6, 2, and 7) is slightly different. In general, the following connection is obvious: the larger the fire, the stronger the shift in the wind speed distribution towards higher values. Especially larger fires (case 7) are related to a very pronounced shift of the whole wind speed PDF by up to 2 m s^{-1} and a significant portion of winds is above 10 m s^{-1}. Compared to the dependency on the fire intensity, the fire size appears to affect more the whole wind speed distribution rather than the wind maximums only. Here, the range of wind velocities exceeding the non-fire limit varies between only 3.2 % in case of the small fire and more than 25 % for the largest fire setup; much more than the variation of the fire intensity (7-21 %). Thus, the increase in the occurrence of wind velocities above the non-fire distribution is more pronounced, although the highest values occur in the more intense fire scenario.

The impacts of the fire shape (Fig. 7d) are a bit more diverse. Comparing the line fires perpendicular (case 8) and parallel (case 9) to the flow direction with the rectangular fire of the same size (case 2), differences in the shape of the fire-influenced

Atmos. Chem. Phys. Discuss., https://doi.org/10.5194/acp-2017-1204
Manuscript under review for journal Atmos. Chem. Phys.
Discussion started: 27 April 2018

wind PDFs stand out. Both wind distributions for the line fire case have a quite similar shape compared to the non-fire distribution, only shifted by roughly 1 m s^{-1} (parallel fire, case 9) or 2 m s^{-1} (perpendicular fire, case 8) towards higher values. This means that the peak winds are stronger in case of a rectangular fire with a more concentrated heat source. But the frequency of occurrence of winds above the non-fire case in total is in case of the perpendicular orientated fire (case 8) with a fraction of 18 % larger compared to a fraction of 12 % for the rectangular shaped fire (case 2). However, the fractions are again much higher than for the parallel orientated line fire (case 9) with less than 5 % above the non-fire case's wind velocities.

The effects of the fire on the near-surface wind fields weaken drastically with increasing distance to the fire area but are often still present due to a downstream transport of fire-related turbulence and momentum. Table 2 provides the fraction of wind velocities larger than the non-fire peak wind velocities (6 m s^{-1}, except of the cases 1 and 3 with 4.5 or 8 m s^{-1}, respectively) for the zones with different distances to the fire region (boxes A-C in Fig. 2). Already in the near-by fire area, box B, the shift of the wind PDFs and occurrence of above-average wind velocities are mostly small or nearly insignificant in case of weak ambient wind winds (case 1) and a smaller fire size (case 6). Only the stronger fire (case 5), the larger fire (case 7), and the perpendicular orientated line fire (case 8) show noteworthy impacts also further ahead of the fire area due to a stronger generation of turbulence, which is transported downstream and can affect the wind field there much more effective than the weaker turbulence of smaller or weaker fires does. A surprising behavior can be observed for the perpendicular orientated line fire (case 8). Here, the strongest impact on the near-surface wind velocity (concerning the peak winds with 8.7 to 8.2 m s^{-1}) does not occur directly around the fire area but further downstream in box B. Furthermore, also the fraction of wind velocities above the non-fire winds is with 5.4 % in box B most pronounced compared to the other setups. Surprisingly, the fraction of wind velocities above the non-fire limit is for most of the fire setups with 1-2 % still enhanced also more than one kilometer away from the fire area (box C).

Since especially the high wind speeds are important for dust emission, the substantial increase in the frequency of occurrence of wind velocities larger than 6 m s^{-1} indicate a strongly increased dust emission potential during wildfires.

5 Discussion with regard to dust emission potential

The analysis of the near-surface wind pattern has already illustrated that wildfires lead, depending on the state of the atmosphere and the fire properties, to a significant increase in the strength and frequency of occurrence of peak wind velocities. To validate the conceptual model of the dust emission via by wildfires modulated wind fields, a simplified approach was used. For the dust emission itself a representative threshold velocity of 6.5 m s^{-1} is applied. The spatial distribution of areas where and how often the threshold velocity of 6.5 m s^{-1} is exceeded is given in Fig. 8 for all case simulations. Considering the non-fire simulation (Fig. 8a, case 0), it becomes evident that the turbulent fluctuations around the mean ambient wind velocity of 3 m s^{-1} lead to an excess of the chosen threshold velocity in rare cases. However, these small areas are randomly distributed over the model domain and at best only once affected by such a high wind velocity, which means that an efficient dust emission cannot be expected. All other simulations show a highly increased occurrence of horizontal wind velocities above the chosen threshold within and around the fire area up to 100 %, whereas the number and spatial extent of such events depend on the chosen setup.

Atmos. Chem. Phys. Discuss., https://doi.org/10.5194/acp-2017-1204
Manuscript under review for journal Atmos. Chem. Phys.
Discussion started: 27 April 2018

Atmospheric Chemistry and Physics Discussions

The frequency of exceeding the threshold velocity of 6.5 m s^{-1} within the most westward 2 km of the model domain is given in Table 3 (first column). The efficiency of generating wind velocities above the threshold intensifies with increasing fire intensity (Fig. 8f, case 5), fire size (Fig. 8h, case 7) and increasing ambient wind velocity (Fig. 8c/d, case 2/3). The extreme case 3 with an average wind velocity of 5 m s^{-1} is already suitable to exceed the threshold velocity of 6.5 m s^{-1} regularly nearly all over the model domain. However, also here the frequency of occurrence of such horizontal peak winds is drastically strengthened in the fire surrounding, suggesting a strongly enhanced dust emission potential there. Since the fire consumes usually the vegetation cover, a mobilization of soil dust particles can take place quite efficiently. Beside the excesses of the threshold velocity in fire surrounding, an interesting behavior occur for the case simulations with an averaged ambient wind velocity of 3 m s^{-1} and a rectangular fire shape (cases 2, 4-7). While during calm ambient wind conditions (Fig. 8b, case 1) the potential of the fire to generate high wind velocities is limited to the direct fire area, zones of increased surface wind velocities have evolved in other setups in some distance to the fire. Pattern of enhanced wind velocity similar to a vortex trail behind an island developed downstream of the fire area, expresses in belts of exceeded threshold velocities occurring north and southward from a virtual extension downstream of the fire center (see Fig. 8c, 8e-h). The evolution of this pattern might be caused by the strong fire updraft acting as an obstacle within the ambient flow, which has to be circumflowed by the winds. The resulting strong turbulence at the edges of the fire updraft propagates downstream and can be mixed downward again, which finally leads to an excess of the chosen threshold velocity also in some distance to the fire area. Provided that suitable surface conditions exist there, the dust emission potential is increased there as well.

Whereas in most of these cases right in front of the fire area, quasi in the lee of the fire updraft, no above-average wind velocities occur, the situation is quite different in case of the perpendicular orientated line fire (Fig. 8i, case 8). Although, the number of excesses of the threshold velocity close to the fire is comparably low, a large area is affected by such events right downstream of the fire area. Since all other parameters are kept constant, the orientation of the fire to the ambient wind flow direction appears to play an important role by increasing the effective surface being prone to wind erosion. The fire heats the lower atmospheric levels on a wide front and modulates the wind pattern there so that a mixing with undisturbed non-fire influenced air masses can occur only much further downstream and the fire-induced turbulence can be transported much more efficient in flow direction. Therefore, this fire setup has the largest area of influence concerning the surface wind pattern. This special feature of case 8 is insofar remarkable as a dust emission potential arises, which is not only directly connected to the fire plume but the emissions can take place also independently and a mixture with combustion aerosol is not always satisfied. Furthermore, the affected area of fire-induced winds increases in this scenario drastically, which means that also dust sources in some distance to the fire area can be affected and activated to emit mineral dust into the atmosphere.

The atmospheric relevance of emitted particles depend strongly on their injection height, which determine interactions with atmospheric properties and the long-range transport. The injection of mineral dust particles into higher atmospheric levels requires beside the excess of a horizontal threshold velocity also a certain vertical wind velocity, essential to transport these particles into higher atmospheric levels. Necessary updraft velocities to lift dust particles in the air based significantly on the particle size and mass. For simplification, sedimentation velocities of representative particle sizes are used to estimate the needed updraft velocities, which must be greater than the sedimentation velocity resulting from gravitational forces to hold

Atmos. Chem. Phys. Discuss., https://doi.org/10.5194/acp-2017-1204
Manuscript under review for journal Atmos. Chem. Phys.
Discussion started: 27 April 2018

Atmospheric Chemistry and Physics Discussions

the particles in the air. The following particle diameters were chosen representatively (Tegen and Fung, 1994), namely d_1 = 1.46 μm (clay), d_2 = 12.2 μm (small silt), d_3 = 36 μm (large silt), d_4 = 76 μm (small sand), and d_5 = 1,000 μm (giant particles, large sand). The corresponding sedimentation velocities v_{sed} of these particle diameters d_1-d_5 result using the calculations with slip and shape correction based on Hinds (1982) in $v_{\mathrm{sed}}(d_1) = 0.00014\,\mathrm{m\,s^{-1}}$, $v_{\mathrm{sed}}(d_2) = 0.009\,\mathrm{m\,s^{-1}}$, $v_{\mathrm{sed}}(d_3) = 0.08\,\mathrm{m\,s^{-1}}$, $v_{\mathrm{sed}}(d_4) = 0.27\,\mathrm{m\,s^{-1}}$, and $v_{\mathrm{sed}}(d_5) = 5.06\,\mathrm{m\,s^{-1}}$. To hold and raise particles of such a size in the atmosphere, these velocities have to be definitely exceeded by the fire or atmospheric updraft velocities. Consequently, they are used here as a simplified estimation of necessary updraft velocities w_1-w_5, which have to be occurring coincidently together with an excess of the threshold velocity to get particles emitted into higher levels of the atmosphere. The probabilities of the occurrence of simultaneous incidences of a horizontal wind velocity above $6.5\,\mathrm{m\,s^{-1}}$ and a updraft velocity w_1-w_5 greater than the calculated sedimentation velocities for the chosen particle diameters are given in Tab. 3 for all case simulations. Representatively for a particle diameter of d_4 = 76 μm, the spatial distribution of the frequency of occurrence of the vertical velocity $w_4 > 0.27\,\mathrm{m\,s^{-1}}$ in the lowest model level is shown in Fig. 9 and the corresponding overlap with areas where the horizontal threshold velocity is exceeded as well (Fig. 8) is shown in Fig. 10. As visible in Fig. 9, a vertical velocity $w_4 > 0.27\,\mathrm{m\,s^{-1}}$ occurs for every grid cell with a frequency of 5-30 % already without any fire influence (cf. Fig. 9a, case 0). However, the impact of the fire leads in general to an increase in the occurrence of such updraft velocities up to 100 % directly above the fire area and also to the formation of an area of enhanced probabilities of occurrence within some hundreds of meters up to 1 km downstream of the fire area. Due to the effect of the ambient wind, the strongest updrafts occur slightly downstream of the actual fire center.

Regions where the horizontal threshold velocity and the updraft velocity w_4 are exceeded simultaneously are shown in Fig. 10. As expected, the suitable zones decrease significantly. For the majority of the cases, only the immediate fire area remains to a large extent suitable for the injection of dust particles up to a size of d_4 = 76 μm into the atmosphere, whereas the intensity and extent of such areas depend again on the fire properties. Larger and more intense fires tend to have a much higher probability to inject dust particles of this size compared to weaker and smaller fires. The behavior of the perpendicular orientated line fire (Fig. 10i, case 8) stands out again, in particular concerning the suitable area of dust uplift. Although no region with constant high updraft velocity exists, the area where horizontal excesses of the threshold velocity occur together with suitable updrafts extends up to 500 m ahead of the original fire line. In total, more than 9 % of the grid cells within the most westward two kilometers of the domain are affected at least once by such a suitable combination, which is by far the highest value apart from case 3 with its high ambient wind velocity. Since such line fires appear to represent a quite realistic scenario for agriculture related grassland fires, the high area of possible regions acting as dust sources also in the larger surrounding of the fire area is remarkable and increase the dust emission potential drastically.

In general, it can be concluded that the combination of sufficient strong horizontal and vertical wind velocities occur quite frequently, especially in fire surroundings, which mean that the fire produce suitable conditions for the injection of dust particles up to a size range of small sand particles (Tab. 3). However, within the fire area the updrafts reach velocities, which are so strong that also dust particles of a size of one millimeter or even larger can be raised and inject into the atmosphere. Although these events are quite rare and limited to the direct fire area, for the majority of the scenarios horizontal wind velocities above the threshold and updrafts with $w_5 > 5.1\,\mathrm{m\,s^{-1}}$ can be observed. Since updraft velocities larger than $10\,\mathrm{m\,s^{-1}}$, with extreme values

reaching nearly 30 m s^{-1} (cf. Tab. 3), always develop above the fire area (cf. Fig. 11) and reaching altitudes of more than 1 km, the in the literature described raise of super-micrometer particles (e.g., Radke, 1991; Nisantzi et al., 2014) can be explained quite well with the development of the strong fire-updraft winds. Contrasting the vertical motions of the fire simulations 20 min after fire ignition in Fig. 11 with that of the non-fire conditions (Fig. 11a, case 0), the fire impacts are evident. Significant updraft velocities derive from the fire convective plume are present close to the fire area and were already transported downstream due to the impacts of the ambient wind. The strong restructuring of the "normal" atmospheric pattern happening after fire ignition within the lower 1-2 km of the atmosphere allows an efficient injection of especially small dust particles with low sedimentation velocities in these altitudes where larger- or synoptic-scale processes, which are not tackled by the setup of this study, can lead to a further transport and distribution within the free atmosphere. Larger particles with much higher sedimentation velocities, by contrast, will start to settle down again already close to the fire area when the fire updraft loses power.

Regarding the intensity of the peak upward motion, all fire simulations have a significant increased vertical velocity, compared to the non-fire simulation by a factor of 3-6. The strongest updrafts were produced at calm conditions (case 1) as well as during more intense (case 5) and larger (case 7) fires. Whereas the connection to fire size and intensity is quite obvious, the comparable updraft velocity under weak background winds is related to the widely absence of downstream drifts so that the upward motion of the heated air can develop much more undisturbed as shown in the vertical profiles in Fig. 6d. Thus, the total emission potential as well as the maximum injection height are assumed to be intensify with increasing fire size and strength, resulting from a more efficient acceleration of the near-surface winds and a stronger updraft velocity and thus a more efficient injection into the free troposphere, while the weaker and smaller fires as well as a stronger ambient velocity lead to lower maximum possible injection heights. However, the fire generated turbulence penetrates always much deeper into the atmosphere than the non-fire turbulence, suggesting an efficient exchange of the fire plume with higher altitudes can take place in each case.

Concerning the total emission potential of wildfires, it becomes clear that it also depends strongly on the ambient wind velocity. In case of stronger ambient winds the likelihood of exceeding the threshold velocity is much higher since already a small intensification of the winds due to the fire is sufficient enough to reach the threshold and mobilize dust particles. Under conditions of high ambient wind velocities the excess of the chosen threshold can occur partly also without any fire-related impacts. Apart of that, an increase in both fire intensity and size enhances the dust emission potential drastically via providing a higher energy release, the development of a stronger updraft and finally a higher acceleration of the near-surface winds can take place. In contrast, small and weak fires result only in a weak increase of the near-surface wind velocities and have a more limited emission potential. But nevertheless, they are able to raise dust particles too and inject them within the atmosphere.

6 Conclusions

The conceptual model how wildfires can act as a source of mineral dust emitted into the atmosphere was analyzed within this study. To quantify the impacts of the so-called pyro-convection, Large-Eddy simulations with ASAM were performed. In total,

9 different model setups were applied to describe varying ambient meteorological wind conditions as well as fire properties representing typical grassland and shrubland fires.

The analysis has shown that the energy released by the fires modulates strongly the near-surface wind velocities and is related to a significant increase in the occurrence of high horizontal wind peaks. These high wind velocities, which are up to 4 m s^{-1} higher than normally in a non-fire influenced PBL occurring wind velocities and have a fraction of up to 100 % in the direct surrounding of the fire area. These strong interaction with lower tropospheric properties and here in particular the occurrence of the high peak winds, which are most crucial for dust mobilization, shows that the potential of mineral dust emissions during wildfires is increased drastically.

While the fire impacts lead to an excess of a wind velocity of 6.5 m s^{-1}, typically sufficient for dust emission, the strength and frequency of occurrence of such peak wind velocities depend strongly on the fire properties. The larger and the more intense the fire, the more pronounced the increase in near-surface wind velocities and consequently the strength of dust mobilization potential are. A quite important parameter appears to be the shape and orientation of a fire to the ambient wind direction. The distribution of the heat source on a broad line perpendicular to the flow direction leads to a much stronger downstream transport of the fire-induced turbulence compared to a more aggregated fire of the same size. This increases the dust emission potential also up to one kilometer and more ahead of the actual fire area, and thus can impact also non-fire related dust sources.

The interplay of the fire with the strength of the ambient wind velocity is impacting the plume characteristics, the possible injection height and the atmospheric transport of once lifted dust particles, which finally determine the atmospheric impacts. Under calm conditions, the fire updraft with the raised participles can penetrate much deeper into the (free) atmosphere, where stronger ambient winds lead rather to a downstream transport of the fire induced air. But nevertheless, the fire plumes of the chosen setups always exceeded the top of the modeled PBL and led to an injection into the free atmosphere, which is crucial for the long-range transport and the interactions with atmospheric properties like radiation budget and cloud microphysics. Smaller and weaker fires show less strong effects on the near-surface winds and a reduced dust emission potential but are still able to raise particles and inject them into the (lower) troposphere where synoptic-scale processes can lead to a further distribution and also to an exchange between the PBL and the free atmosphere.

Since the outcomes of this study illustrate that wildfires have a strong potential of favoring the emission of mineral dust by modifying the near-surface winds, an implementation of the fire-related dust emission process in meso-scale atmosphere-aerosol models is necessary to achieve a more accurate estimation of the total dust load and dust-associated impacts on radiation budget, cloud and precipitation formation processes especially on larger spatial scales. Since these models cannot resolve directly the fire-related turbulence, responsible for dust entrainment, the development of a parameterization of the process is necessary. Therefore, the results gained here can be used to derive a relation between the fire properties and the resulting modulations of the wind speed distribution, which can be applied afterwards in a dust emission scheme to determine the strength of the fire-related dust emission fluxes. To describe this process and the subsequent atmospheric fire-driven pathways as accurate as possible, additional information on basic fire properties (e.g., fire radiative power, fire size) and land characteristics (e.g., soil type, vegetation cover) are required, which can be obtained from satellite products for wildfire monitoring and land

cover maps. Using that, a comparison of the modeled fire-related dust emission with airborne or remote sensing measurements of the dust content in smoke plumes become possible.

This study gives a first introduction into the dust emission process during wildfires. Further quantification will allow for an estimation of the amount of fire-related dust emissions at a continental or global scale and can finally contribute to a reduction of the uncertainty in the aerosol-climate feedback, especially regarding the highly variable anthropogenic part, the main cause of wildfires.

Acknowledgements. R.W. and K.S. acknowledge the Leibniz Association funding for the project "Dust at the interface - modelling and remote sensing". We acknowledge the Centre for Information Services and High Performance Computing (ZIH) of the Technische Universität Dresden (TU Dresden) for providing computing capacity.

References

Albalasmeh, A. A., Berli, M., Shafer, D. S., and Ghezzehei, T. A.: Degradation of moist soil aggregates by rapid temperature rise under low intensity fire, Plant and soil, 362, 335-344, 2013.

Alves, C. A., Gonçalves, C., Pio, C. A., Mirante, F., Caseiro, A., Tarelho, L., Freitas, M. C., and Viegas, D. X.: Smoke emissions from biomass burning in a Mediterranean shrubland, Atmospheric Environment, 44, 3024-3033, 2010.

Amiridis, V., Giannakaki, E., Balis, D. S., Gerasopoulos, E., Pytharoulis, I., Zanis, P., Kazadzis, S., Melas, D., and Zerefos, C.: Smoke injection heights from agricultural burning in Eastern Europe as seen by CALIPSO, Atmospheric Chemistry and Physics, 10, 11567-11576, 10.5194/acp-10-11567-2010, 2010.

Andela, N., Morton, D. C., Giglio, L., Chen, Y., van der Werf, G. R., Kasibhatla, P. S., DeFries, R. S., Collatz, G. J., Hantson, S., Kloster, S., Bachelet, D., Forrest, M., Lasslop, G., Li, F., Mangeon, S., Melton, J. R., Yue, C., and Bachelet, D.: A human-driven decline in global burned area. Science, 356(6345), 1356-1362, 2017.

Ansmann, A., Baars, H., Tesche, M., Müller, D., Althausen, D., Engelmann, R., Pauliquevis, T., and Artaxo, P.: Dust and smoke transport from Africa to South America: Lidar profiling over Cape Verde and the Amazon rainforest, Geophysical Research Letters, 36, 10.1029/2009gl037923, 2009.

Cachier, H., Liousse, C., Buat-Menard, P., and Gaudichet, A.: Particulate content of savanna fire emissions, Journal of Atmospheric Chemistry, 22, 123-148, 1995.

Chalbot, M. C., Nikolich, G., Etyemezian, V., Dubois, D. W., King, J., Shafer, D., Gamboa da Costa, G., Hinton, J. F., and Kavouras, I. G.: Soil humic-like organic compounds in prescribed fire emissions using nuclear magnetic resonance spectroscopy, Environmental pollution, 181, 167-171, 10.1016/j.envpol.2013.06.008, 2013.

Clark, T. L., Radke, L., Coen, J., and Middleton, D.: Analysis of small-scale convective dynamics in a crown fire using infrared video camera imagery, Journal of Applied Meteorology, 38, 1401-1420, 1999.

Clements, C. B., Zhong, S., Goodrick, S., Li, J., Potter, B. E., Bian, X., Heilman, W. E., Charney, J. J., Perna, R., Jang, M., Lee, D., Patel, M., Street, S., and Aumann, G.: Observing the dynamics of wildland grass fires: Fireflux – a field validation experiment, Bulletin of the American Meteorological Society, 88, 1369-1382, 2007.

Clements, C. B., Zhong, S., Bian, X., Heilman, W. E., and Byun, D. W.: First observations of turbulence generated by grass fires, Journal of Geophysical Research, 113, 10.1029/2008jd010014, 2008.

Coen, J., Mahalingam, S., and Daily, J.: Infrared imagery of crown-fire dynamics during FROSTFIRE, Journal of Applied Meteorology, 43, 1241-1259, 2004.

Coen, J. L., Cameron, M., Michalakes, J., Patton, E. G., Riggan, P. J., and Yedinak, K. M.: WRF-Fire: coupled weather-wildland fire modeling with the weather research and forecasting model, Journal of Applied Meteorology and Climatology, 52, 16-38, 2013.

Cunningham, P., and Linn, R. R.: Numerical simulations of grass fires using a coupled atmosphere-fire model: Dynamics of fire spread, Journal of Geophysical Research, 112, 10.1029/2006jd007638, 2007.

Diapouli, E., Popovicheva, O., Kistler, M., Vratolis, S., Persiantseva, N., Timofeev, M., Kasper-Giebl, A., and Eleftheriadis, K.: Physico-chemical characterization of aged biomass burning aerosol after long-range transport to Greece from large scale wildfires in Russia and surrounding regions, Summer 2010, Atmospheric environment, 96, 393-404, 2014.

Frankman, D., Webb, B. W., Butler, B. W., Jimenez, D., Forthofer, J. M., Sopko, P., Shannon, K. S., Hiers, J. K., and Ottmar, R. D.: Measurements of convective and radiative heating in wildland fires, International Journal of Wildland Fire, 22, 157-167, 2013.

Fromm, M., Lindsey, D. T., Servranckx, R., Yue, G., Trickl, T., Sica, R., Doucet, P., and Godin-Beekmann, S.: The untold story of pyrocumulonimbus, Bulletin of the American Meteorological Society, 91(9), 1193-1209, 2010.

Gatebe, C. K., Ichoku, C. M., Poudyal, R., Roman, M. O., and Wilcox, E.: Surface albedo darkening from wildfires in northern sub-Saharan Africa, Environmental Research Letters, 9, 065003, 10.1088/1748-9326/9/6/065003, 2014.

Gaudichet, A., Echalar, F., Chatenet, B., Quisefit, J. P., Malingre, G., Cachier, H., Buat-Menard, P., Artaxo, P., and Maenhaut, W.: Trace elements in tropical African savanna biomass burning aerosols, Journal of Atmospheric Chemistry, 22, 19-39, 1995.

Hand, V. L., Capes, G., Vaughan, D. J., Formenti, P., Haywood, J. M., and Coe, H.: Evidence of internal mixing of African dust and biomass burning particles by individual particle analysis using electron beam techniques, Journal of Geophysical Research, 115, 10.1029/2009jd012938, 2010.

Haywood, J. M., Pelon, J., Formenti, P., Bharmal, N., Brooks, M., Capes, G., Chazette, P., Chou, C., Christopher, S., Coe, H., Cuesta, J., Derimian, Y., Desboeufs, K., Greed, G., Harrison, M., Heese, B., Highwood, E. J., Johnson, B., Mallet, M., Marticorena, B., Marsham, J., Milton, S., Myhre, G., Osborne, S. R., Parker, D. J., Rajot, J. L., Schulz, M., Slingo, A., Tanré, D., and Tulet, P.: Overview of the Dust and Biomass-burning Experiment and African Monsoon Multidisciplinary Analysis Special Observing Period-0, Journal of Geophysical Research, 113, 10.1029/2008jd010077, 2008.

Hinds, W. C.: Aerosol technology: properties, behavior, and measurement of airborne particles. A Wiley-Interscience Publication John Wiley & Sons, 504pp., 1982.

Jähn, M., Knoth, O., König, M., and Vogelsberg, U.: ASAM v2.7: a compressible atmospheric model with a Cartesian cut cell approach, Geosci. Model Dev., 8, 317-340, doi:10.5194/gmd-8-317-2015, 2015.

Jähn, M., Muñoz Esparza, D., Chouza, F., Reitebuch, O., Knoth, O., Haarig, M., and Ansmann, A.: Investigations of boundary layer structure, cloud characteristics and vertical mixing of aerosols at Barbados with large eddy simulations, Atmos. Chem. Phys., 16, 651-674, 2016.

Johnson, B. T., Heese, B., McFarlane, S. A., Chazette, P., Jones, A., and Bellouin, N.: Vertical distribution and radiative effects of mineral dust and biomass burning aerosol over West Africa during DABEX, Journal of Geophysical Research, 113, 10.1029/2008jd009848, 2008.

Kalma, J. D., Speight, J. G., and Wasson, R. J.: Potential wind erosion in Australia: A continental perspective. International Journal of Climatology, 8(4), 411-428, 1988.

Kavouras, I. G., Nikolich, G., Etyemezian, V., DuBois, D. W., King, J., and Shafer, D.: In situ observations of soil minerals and organic matter in the early phases of prescribed fires, Journal of Geophysical Research: Atmospheres, 117, D12313, 2012.

Keeley, J. E., Fotheringham, C. J., and Morais, M.: Reexamining fire suppression impacts on brushland fire regimes, Science, 284(5421), 1829-1832, 1999.

Kok, J. F., Parteli, E. J. R., Michaels, T. I., and Karam, D. B.: The physics of wind-blown sand and dust, Reports on Progress in Physics, 75, 106901, 2012.

Knoth, O. and Wensch, J.: Generalized split-explicit Runge-Kutta methods for the compressible Euler equations, Mon. Weather Rev., 142, 2067-2081, 2014.

Lareau, N. P. and Clements, C. B.: The Mean and Turbulent Properties of a Wildfire Convective Plume, Journal of Applied Meteorology and Climatology, 56, 2289-2299, 2017.

Levin, Z., Ganor, E., and Gladstein, V.: The effects of desert particles coated with sulfate on rain formation in the eastern Mediterranean, Journal of Applied Meteorology, 35, 1511-1523, 1996.

Linn, R. R., and Cunningham, P.: Numerical simulations of grass fires using a coupled atmosphere-fire model: Basic fire behavior and dependence on wind speed, Journal of Geophysical Research, 110, 10.1029/2004jd005597, 2005.

Maenhaut, W., Salma, I., Cafmeyer, J., Annegarn, H. J., and Andreae, M. O., Regional atmospheric aerosol composition and sources in the eastern Transvaal, South Africa, and impact of biomass burning, Journal of Geophysical Research: Atmospheres, 101, 23631-23650, 1996.

Marticorena, B., and Bergametti, G.: Modeling the atmospheric dust cycle: 1. Design of a soil-derived dust emission scheme, Journal of Geophysical Research: Atmospheres, 100(D8), 16415-16430, 1995.

Maudlin, L. C., Wang, Z., Jonsson, H. H., and Sorooshian, A.: Impact of wildfires on size-resolved aerosol composition at a coastal California site, Atmospheric Environment, 119, 59-68, 2015.

McCluskey, C. S., DeMott, P. J., Prenni, A. J., Levin, E. J., McMeeking, G. R., Sullivan, A. P., Hill, T. C. J., Nakao, S., Carrico, C. M., and Kreidenweis, S. M.: Characteristics of atmospheric ice nucleating particles associated with biomass burning in the US: Prescribed burns and wildfires, Journal of Geophysical Research: Atmospheres, 119, 10458-10470, 10.1002/2014JD021980, 2014.

Mell, W., Charney, J., Jenkins, M. A., Cheney, P., and Gould, J.: Numerical simulations of grassland fire behavior from the LANL-FIRETEC and NIST-WFDS models, In Remote Sensing and Modeling Applications to Wildland Fires (pp. 209-225), Springer Berlin Heidelberg, 2008.

Merino-Martín, L., Field, J. P., Villegas, J. C., Whicker, J. J., Breshears, D. D., Law, D. J., and Urgeghe, A. M.: Aeolian sediment and dust fluxes during predominant "background" wind conditions for unburned and burned semiarid grassland: Interplay between particle size and temporal scale, Aeolian Research, 14, 97-103, 2014.

Morvan, D.: Physical phenomena and length scales governing the behaviour of wildfires: a case for physical modelling. Fire technology, 47, 437-460, 2009.

Nisantzi, A., Mamouri, R. E., Ansmann, A., and Hadjimitsis, D.: Injection of mineral dust into the free troposphere during fire events observed with polarization lidar at Limassol, Cyprus, Atmospheric Chemistry and Physics, 14, 12155-12165, 10.5194/acp-14-12155-2014, 2014.

Paris, R., Desboeufs, K. V., Formenti, P., Nava, S., and Chou, C.: Chemical characterisation of iron in dust and biomass burning aerosols during AMMA-SOP0/DABEX: implication for iron solubility, Atmospheric Chemistry and Physics, 10, 4273-4282, 10.5194/acp-10-4273-2010, 2010.

Palmer, T. Y.: Large fire winds, gases and smoke, Atmospheric Environment, 15, 2079-2090, 1981.

Pio, C. A., Legrand, M., Alves, C. A., Oliveira, T., Afonso, J., Caseiro, A., Puxbaum, H., Sanchez-Ochoa, A., and Gelencsér, A.: Chemical composition of atmospheric aerosols during the 2003 summer intense forest fire period, Atmospheric Environment, 42, 7530-7543, 2008.

Radke, L. F., Hegg, D. A., Hobbs, P. V., Nance, J. D., Lyons, J. H., Laursen, K. K., Weiss, R. E., Riggan, P. J., and Ward, D. E.: Particulate and trace gas emissions from large biomass fire in North America, In Levine, J.S. (ed.) Global Biomass Burning: Atmospheric, Climatic, and Biospheric Implications. The MIT Press, Cambridge, Massachusetts. pp. 209-216, 1991.

Reid, J. S., Koppmann, R., Eck, T. F., and Eleuterio, D. P.: A review of biomass burning emissions part II: intensive physical properties of biomass burning particles, Atmospheric Chemistry and Physics, 5, 799-825, 2005.

Roberts, G., Wooster, M. J., and Lagoudakis, E.: Annual and diurnal African biomass burning temporal dynamics, Biogeosciences, 6(5), 2009.

Schlosser, J. S., Braun, R. A., Bradley, T., Dadashazar, H., MacDonald, A. B., Aldhaif, A. A., Aghdam, M. A., Mardi, A. H., Peng, X., and Sorooshian, A.: Analysis of aerosol composition data for western United States wildfires between 2005 and 2015: Dust emissions, chloride depletion, and most enhanced aerosol constituents; Journal of Geophysical Research: Atmospheres, 122, 8951-8966, 2017.

Shao, Y.: A model for mineral dust emission, Journal of Geophysical Research: Atmospheres, 106(D17), 20239-2025, 2001.

Sun, R., Krueger, S. K., Jenkins, M. A., Zulauf, M. A., and Charney, J. J.: The importance of fire-atmosphere coupling and boundary-layer turbulence to wildfire spread, International Journal of Wildland Fire, 18, 50-60, 2009.

Susott, R. A., Ward, D. E., Babbitt, R. E., and Latham, D. J.: The measurement of trace emissions and combustion characteristics for a mass fire, In: Levine, J. S., ed. Global biomass buring: Atmospheric, climatic, and biosphere implications. Cambridge, MA: MIT Press. p. 245-257., 1991.

Tegen, I., and Fung, I.: Modeling of mineral dust in the atmosphere: Sources, transport, and optical thickness, Journal of Geophysical Research: Atmospheres, 99, 22897-22914, 1994.

Tegen, I., Schepanski, K., and Heinold, B.: Comparing two years of Saharan dust source activation obtained by regional modelling and satellite observations, Atmospheric Chemistry and Physics, 13, 2381-2390, 10.5194/acp-13-2381-2013, 2013.

Veira, A., Kloster, S., Wilkenskjeld, S., and Remy, S.: Fire emission heights in the climate system - Part 1: Global plume height patterns simulated by ECHAM6-HAM2, Atmospheric Chemistry and Physics, 15, 7155-7171, 10.5194/acp-15-7155-2015, 2015.

Wagner, R., Schepanski, K., Heinold, B., and Tegen, I.: Interannual variability in the Saharan dust source activation-Toward understanding the differences between 2007 and 2008, Journal of Geophysical Research: Atmospheres, 121, 4538-4562, 10.1002/2015jd024302, 2016.

Winton, V. H. L., Edwards, R., Bowie, A. R., Keywood, M., Williams, A. G., Chambers, S., Selleck, P. W., Desservettaz, M., Mallet, M., and Paton-Walsh, C.: Dry season aerosol iron solubility in tropical northern Australia, Atmospheric Chemistry and Physics Discussions, 1-32, 10.5194/acp-2016-419, 2016.

Atmos. Chem. Phys. Discuss., https://doi.org/10.5194/acp-2017-1204
Manuscript under review for journal Atmos. Chem. Phys.
Discussion started: 27 April 2018

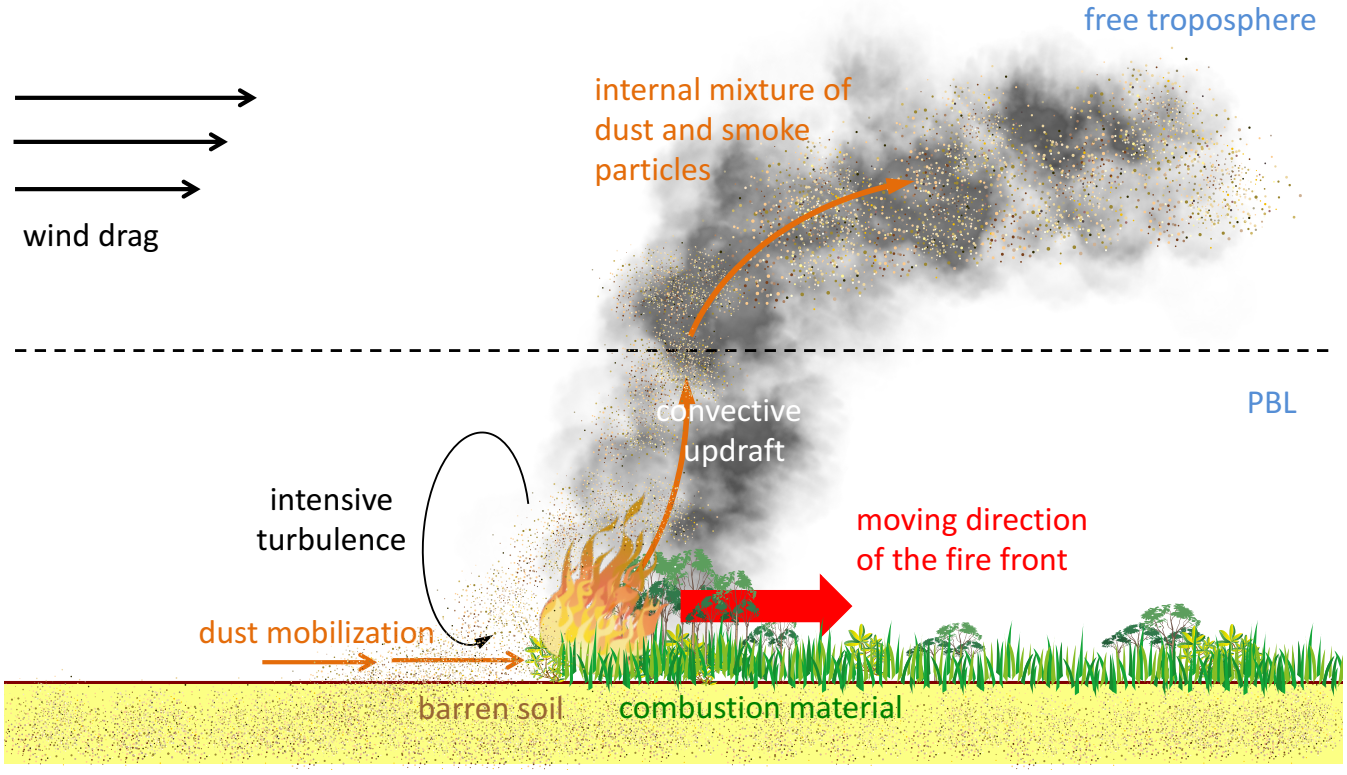

Figure 1. Schematic overview of the processes related to dust emissions during wildfires.

Atmos. Chem. Phys. Discuss., https://doi.org/10.5194/acp-2017-1204
Manuscript under review for journal Atmos. Chem. Phys.
Discussion started: 27 April 2018

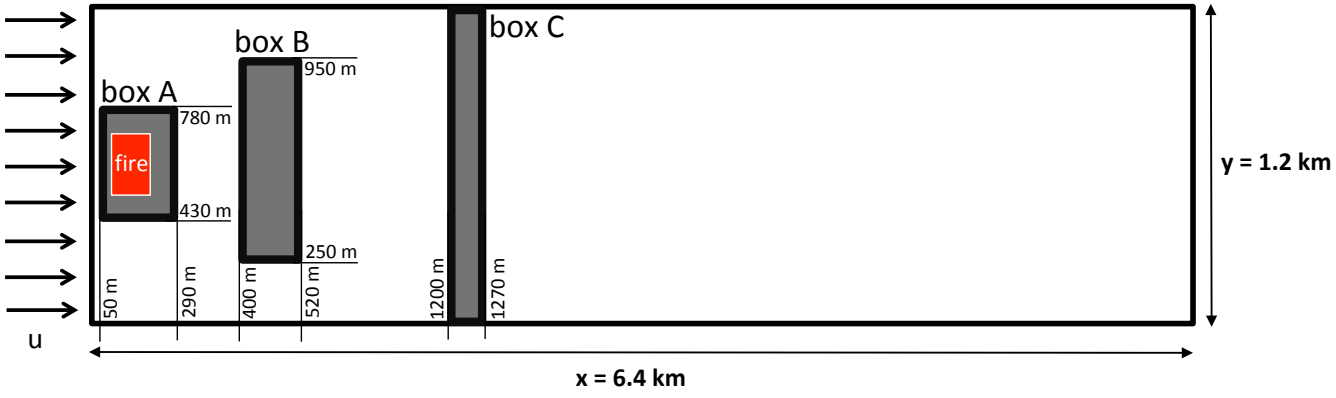

Figure 2. Schematic view of the *x*-*y*-plane of the model domain. Three areas with different distances to the fire area are marked (box A, B, C). Each box has a base size of 84,000 m^2 (Figure not true to scale).

Atmos. Chem. Phys. Discuss., https://doi.org/10.5194/acp-2017-1204
Manuscript under review for journal Atmos. Chem. Phys.
Discussion started: 27 April 2018

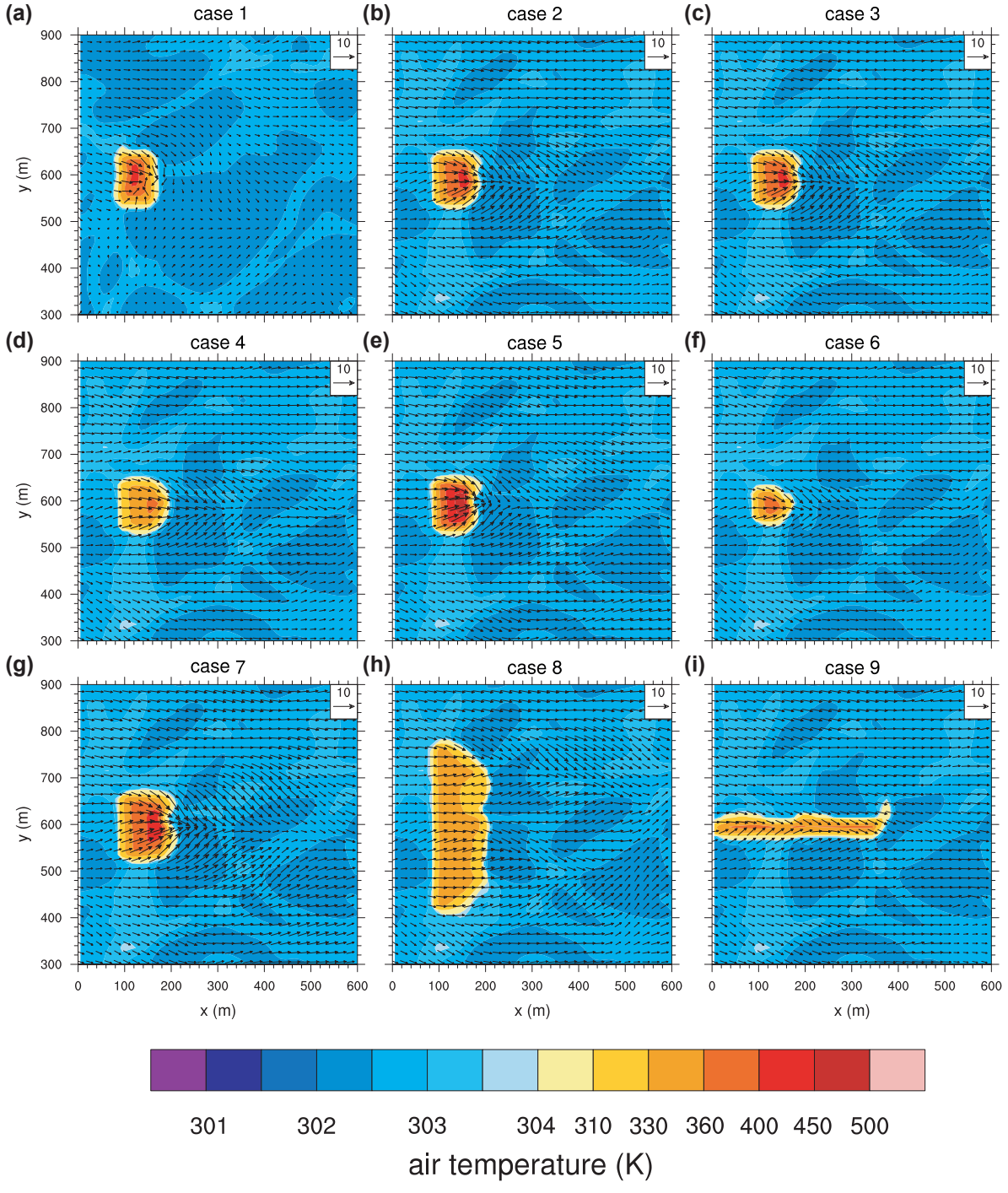

Figure 3. Horizontal cross sections of the wind vector and air temperature fields 20 minutes after fire ignition in the lowest model level of $z = 5$ m.

Atmos. Chem. Phys. Discuss., https://doi.org/10.5194/acp-2017-1204
Manuscript under review for journal Atmos. Chem. Phys.
Discussion started: 27 April 2018

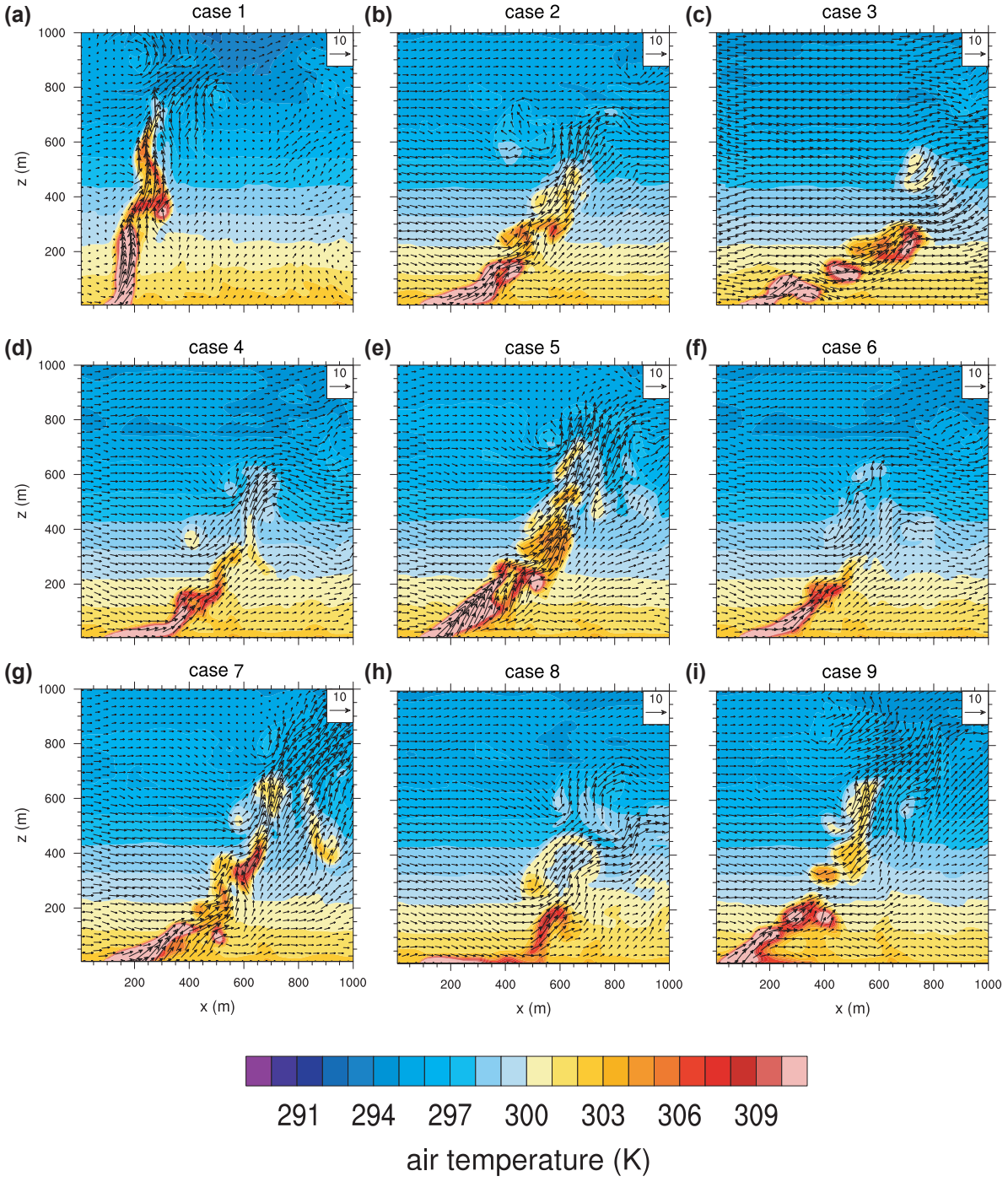

Figure 4. Vertical cross sections of the wind vector and air temperature fields trough the fire center ($y = 600$ m) 20 minutes after fire ignition.

Atmos. Chem. Phys. Discuss., https://doi.org/10.5194/acp-2017-1204
Manuscript under review for journal Atmos. Chem. Phys.
Discussion started: 27 April 2018

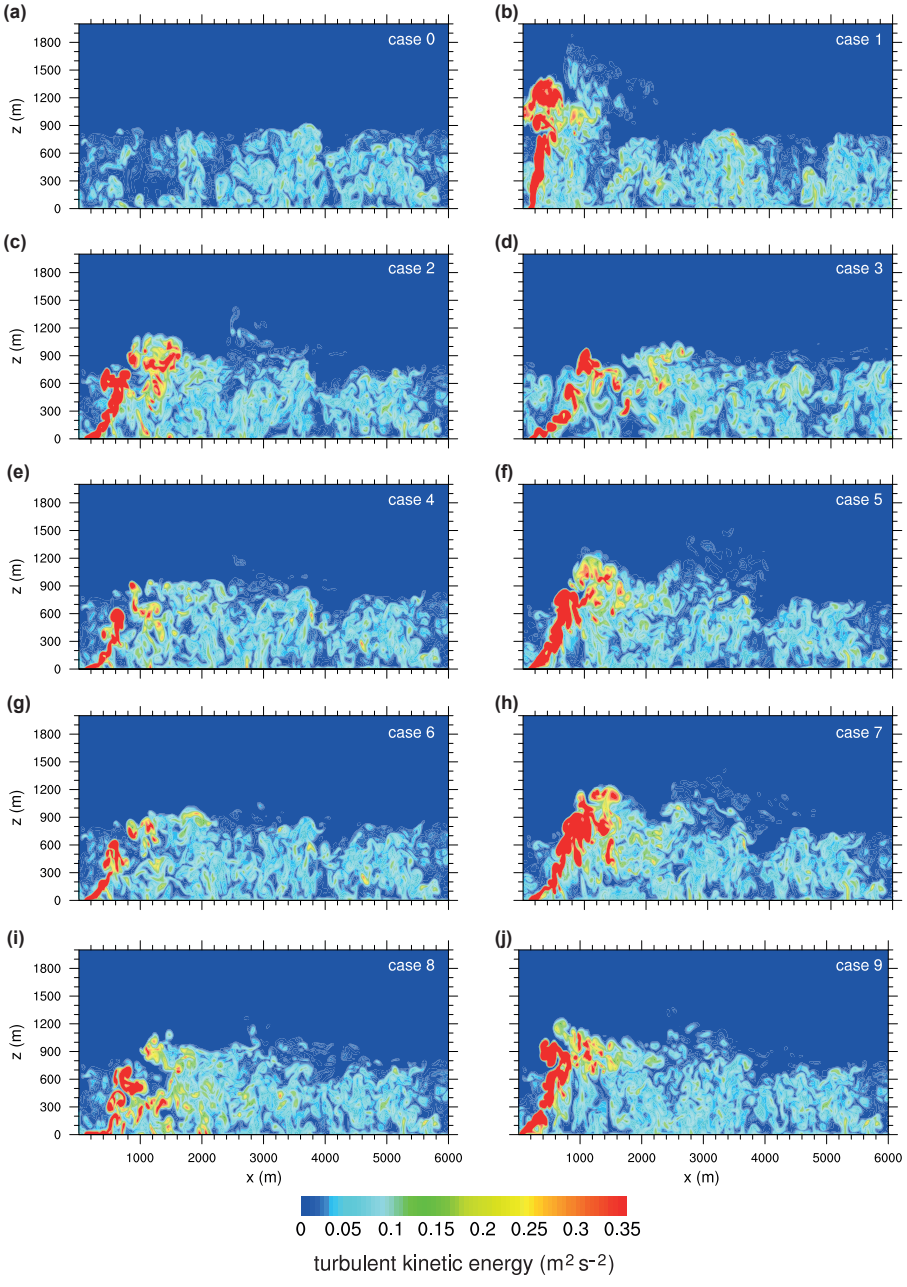

Figure 5. Vertical cross sections of the turbulent kinetic energy (TKE) trough the fire center ($y = 600$ m) for all case simulations including the non-fire simulation (case 0) 20 minutes after fire ignition.

Atmos. Chem. Phys. Discuss., https://doi.org/10.5194/acp-2017-1204
Manuscript under review for journal Atmos. Chem. Phys.
Discussion started: 27 April 2018

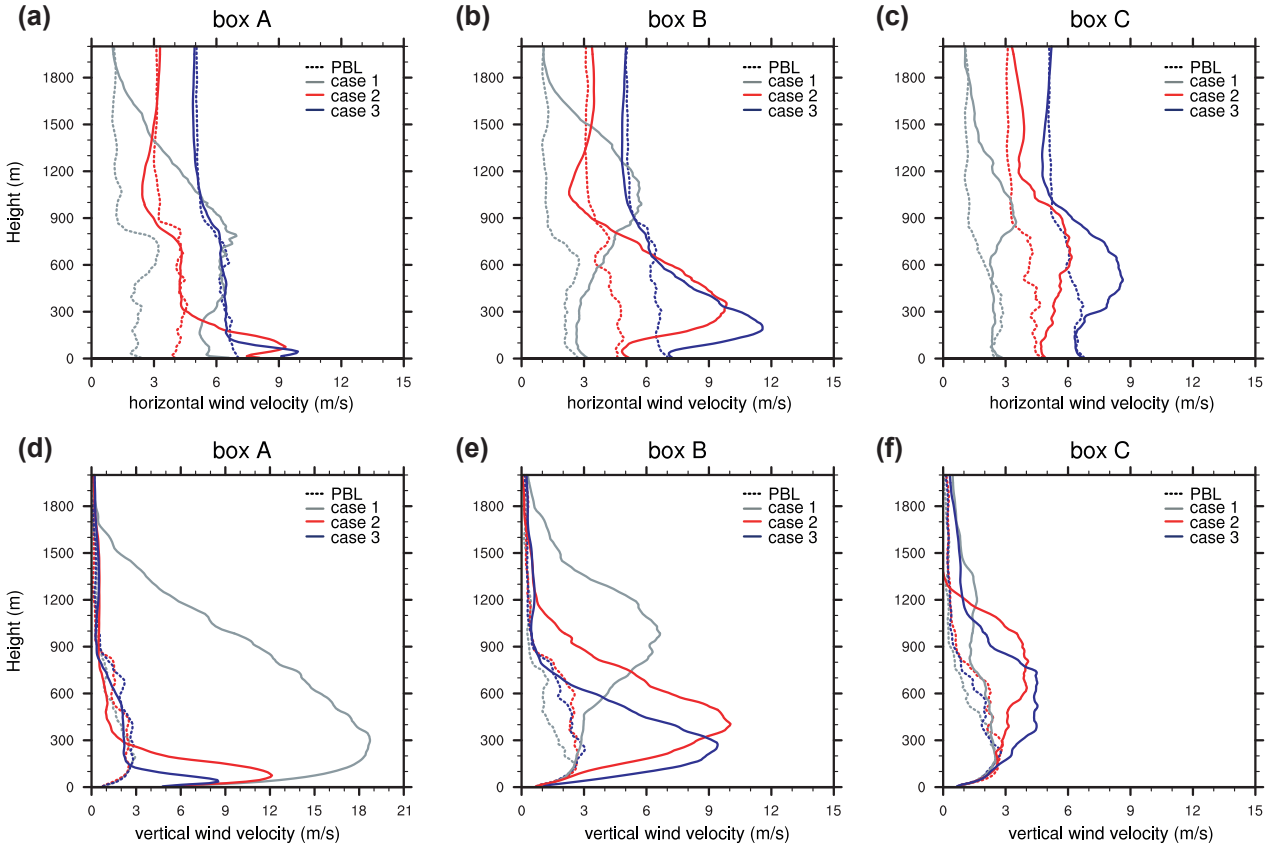

Figure 6. Vertical profiles of the horizontal (upper row) and vertical (lower row) wind velocity for the case simulations 1-3 and different distances to the fire (box A, B, C in Fig. 2). Shown are the atmospheric profiles after fire ignition (solid line) with the profile in the undisturbed non-fire PBL (dashed line). Plotted are means of the maximum values per time step.

Atmos. Chem. Phys. Discuss., https://doi.org/10.5194/acp-2017-1204
Manuscript under review for journal Atmos. Chem. Phys.
Discussion started: 27 April 2018

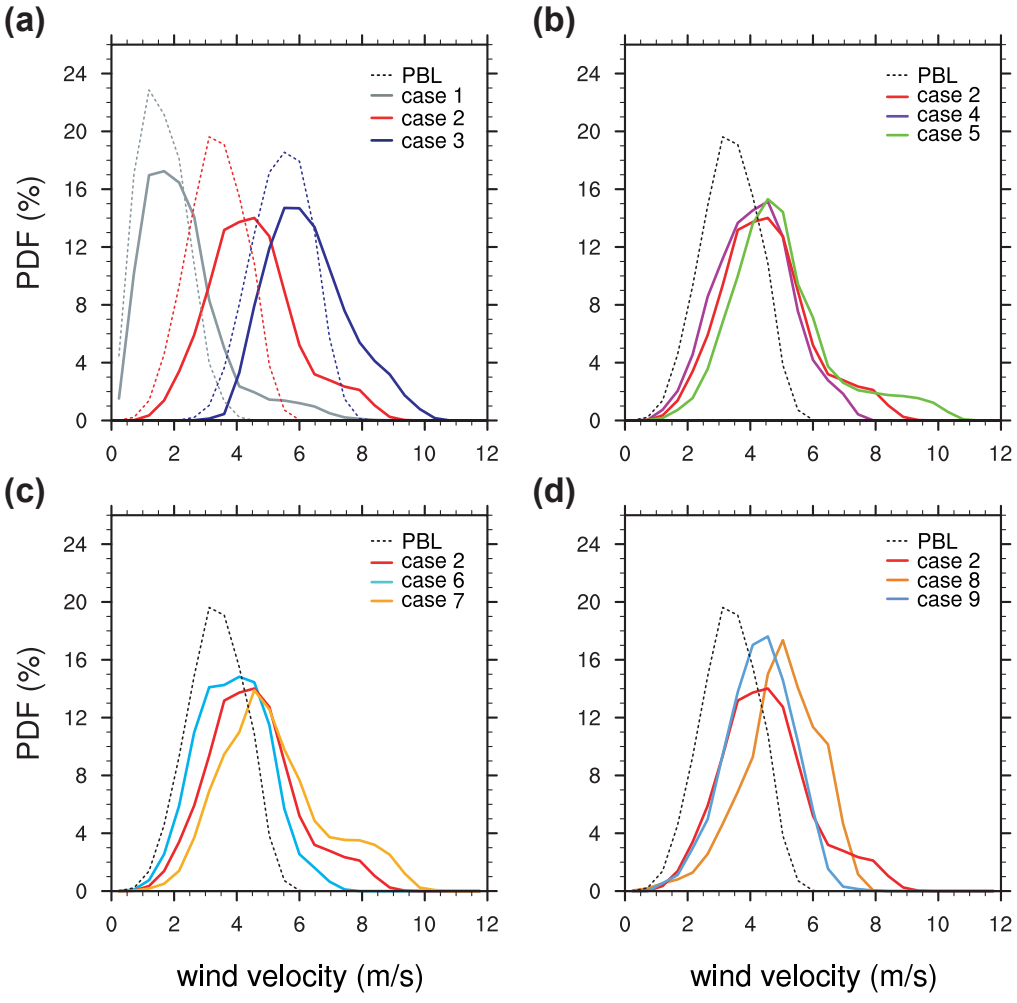

Figure 7. PDFs of the near-surface wind velocity around the fire area (box A) for the different case simulations (solid lines) with respect to the PDFs of the non-fire PBL (dashed lines). (a) compares the impacts of different ambient wind velocity, (b) the impacts of the fire intensity, (c) the impacts of fire size, (d) the impacts of the fire shape - always with respect to the reference case 2.

Atmos. Chem. Phys. Discuss., https://doi.org/10.5194/acp-2017-1204
Manuscript under review for journal Atmos. Chem. Phys.
Discussion started: 27 April 2018

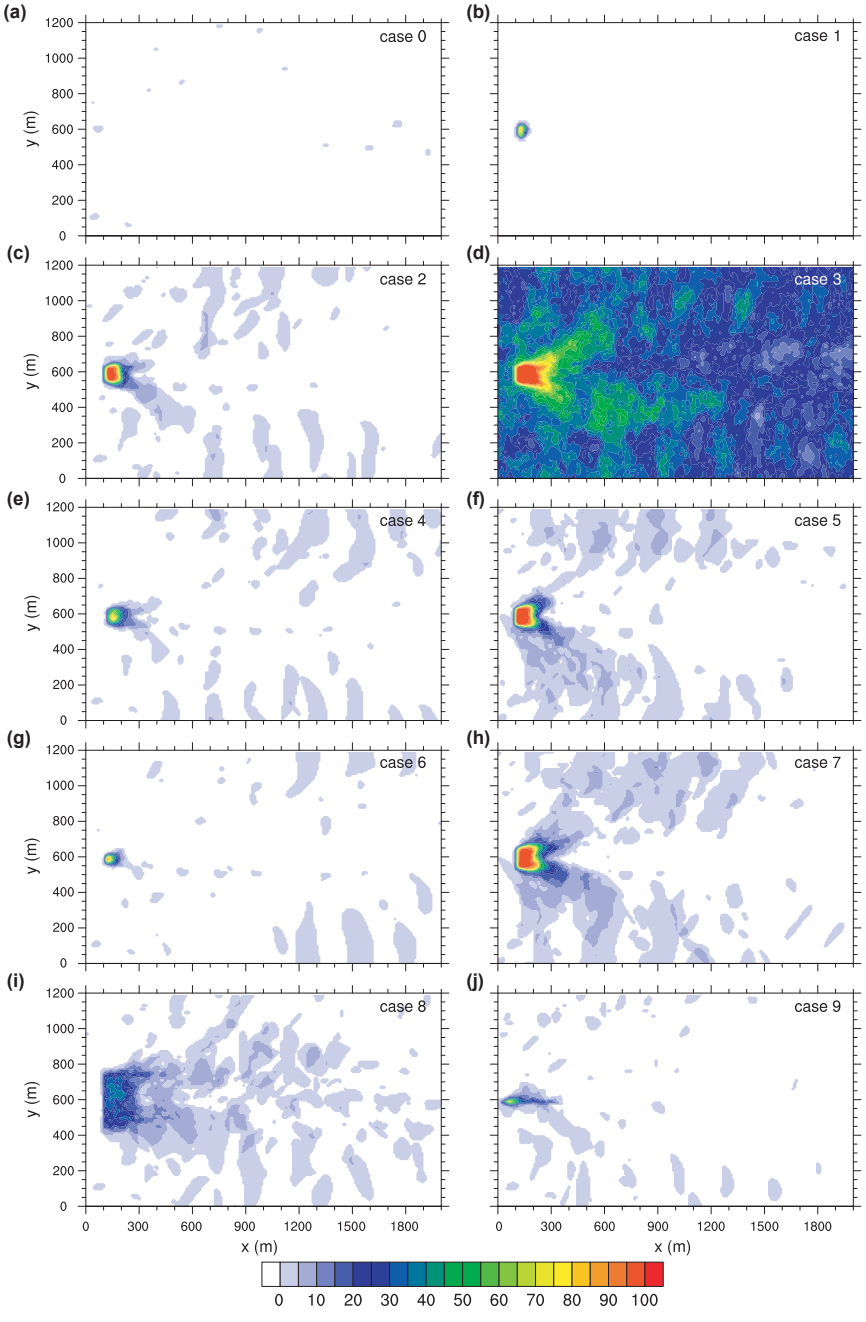

Figure 8. Spatial distribution of areas where a typical threshold velocity v_{tres} of 6.5 m s^{-1} is exceed in lowest model level. Shown is the frequency of occurrence of such wind velocities per grid cell.

Atmos. Chem. Phys. Discuss., https://doi.org/10.5194/acp-2017-1204
Manuscript under review for journal Atmos. Chem. Phys.
Discussion started: 27 April 2018

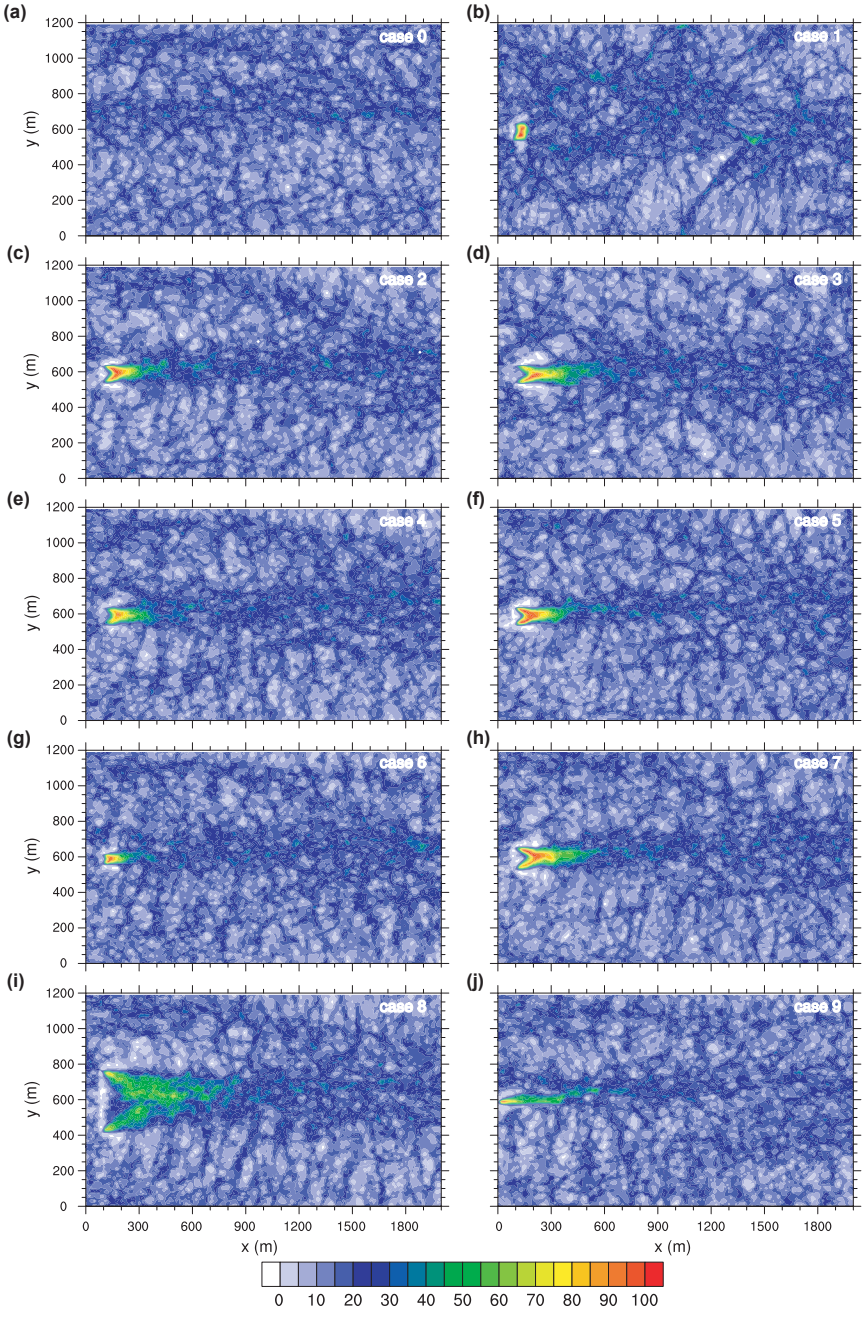

Figure 9. Spatial distribution of areas where the vertical wind velocity w_4 is greater than 0.27 m s^{-1}. Shown is the frequency of occurrence of such updraft velocities per grid cell.

Atmos. Chem. Phys. Discuss., https://doi.org/10.5194/acp-2017-1204
Manuscript under review for journal Atmos. Chem. Phys.
Discussion started: 27 April 2018

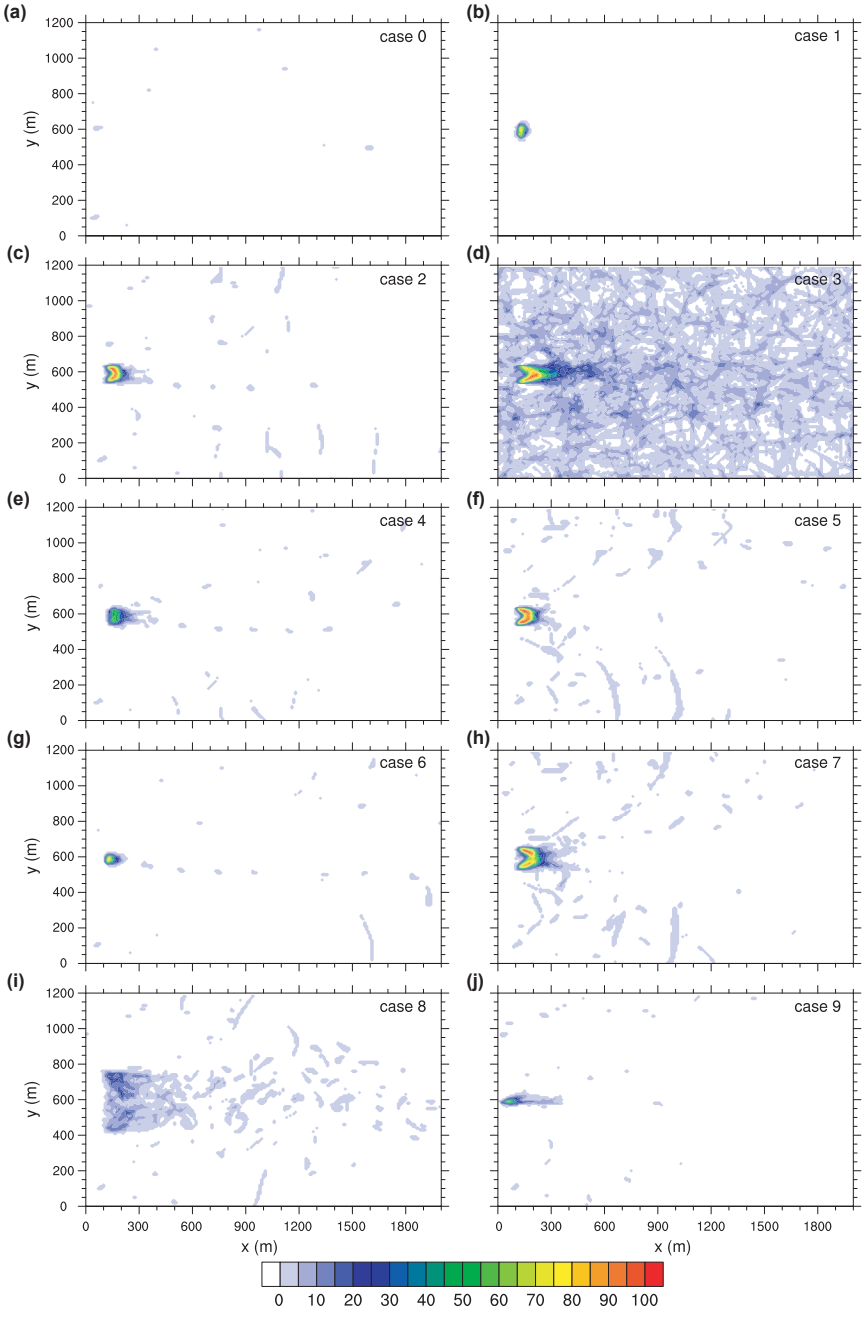

Figure 10. Spatial distribution of areas where both the horizontal threshold velocity $v_{\mathrm{tres}} = 6.5\,\mathrm{m\,s^{-1}}$ (cf. 9) and a vertical wind velocity w_4 greater than $0.27\,\mathrm{m\,s^{-1}}$ (cf. 10) are exceeded at the same time. Shown is the frequency of occurrence of such events per grid cell.

Atmos. Chem. Phys. Discuss., https://doi.org/10.5194/acp-2017-1204
Manuscript under review for journal Atmos. Chem. Phys.
Discussion started: 27 April 2018

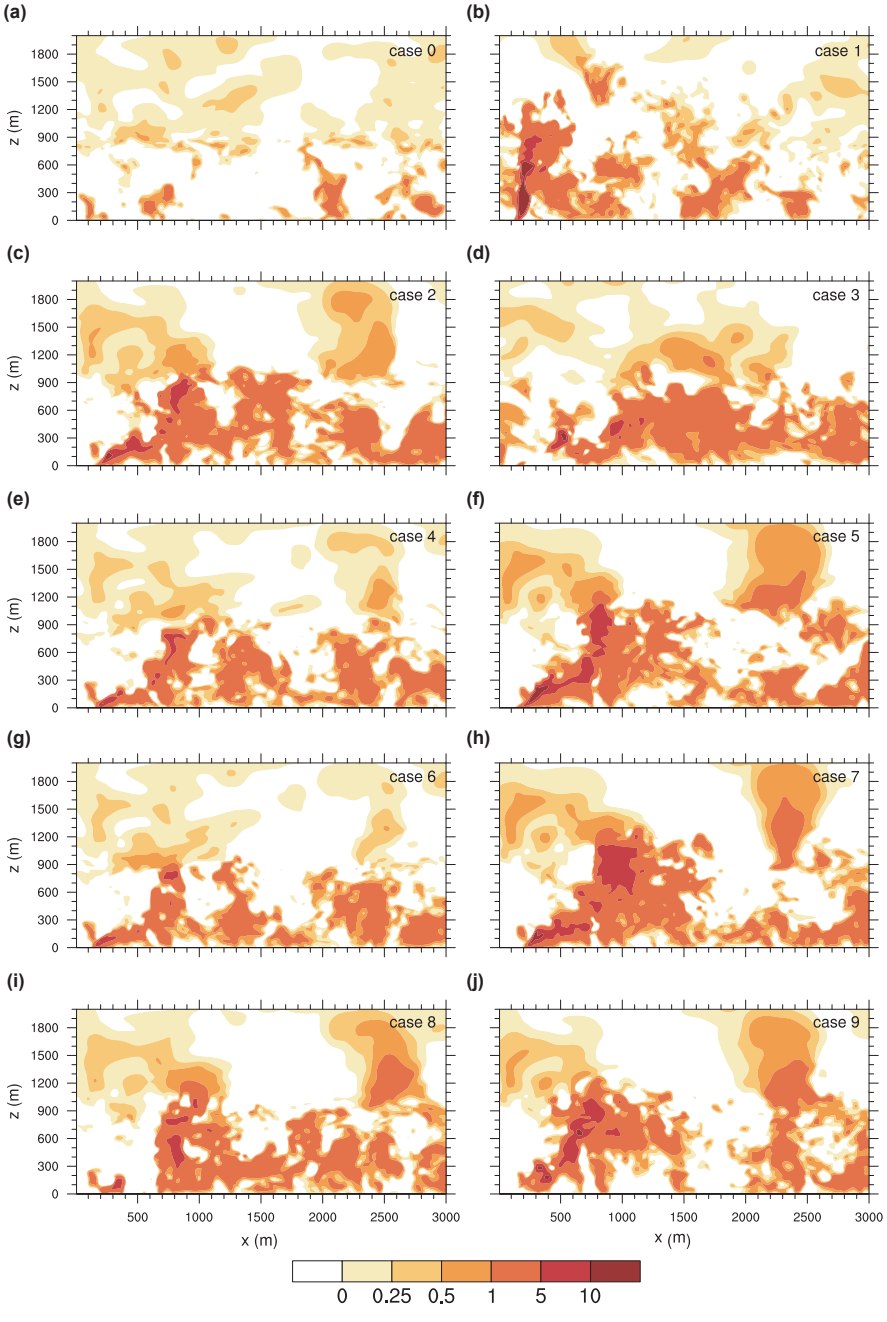

Figure 11. Vertical cross sections of the vertical wind velocity w trough the fire center ($y = 600$ m) for all case simulations including the non-fire simulation (case 0) 20 minutes after fire ignition.

Atmos. Chem. Phys. Discuss., https://doi.org/10.5194/acp-2017-1204
Manuscript under review for journal Atmos. Chem. Phys.
Discussion started: 27 April 2018

Atmospheric Chemistry and Physics Discussions

Table 1. Overview of the case studies.

case	$\lvert v_{10m}\rvert$ (m s^{-1})	F_{fire} (kW m^{-2})	T_{fire} (°C)	A_{fire} (m^2)	fire shape	description
0	3	-	-	-	-	control run (no fire)
1	1	150	1000	7000 = 70x100	rectangular	weak wind conditions
2	3	150	1000	7000 = 70x100	rectangular	moderate wind conditions
3	5	150	1000	7000 = 70x100	rectangular	strong wind conditions
4	3	75	800	7000 = 70x100	rectangular	weaker fire
5	3	270	1200	7000 = 70x100	rectangular	stronger fire
6	3	150	1000	1800 = 40x60	rectangular	smaller fire
7	3	150	1000	11700 = 90x130	rectangular	larger fire
8	3	150	1000	7000 = 20x350	"line" (|)	line fire (perpendicular)
9	3	150	1000	7000 = 350x20	"line" (–)	line fire (parallel)

Atmos. Chem. Phys. Discuss., https://doi.org/10.5194/acp-2017-1204
Manuscript under review for journal Atmos. Chem. Phys.
Discussion started: 27 April 2018

Atmospheric Chemistry and Physics Discussions

Table 2. Fraction of the wind velocities larger than the non-fire limit for the three boxes A, B, and C with different distances to the fire area (cf. Fig. 2). For the majority of the cases with an ambient wind velocity of 3 m s^{-1}, this threshold lies at 6 m s^{-1} (frequency of occurrence > 99.99 %). For both setups with a weaker (case 1) and a higher (case 3) ambient wind velocity, different threshold values of 4.5 and 8 m s^{-1} are used. Additionally, the fractions concerning the 6 m s^{-1}-limit are here indicated in brackets too.

case	description	box A	box B	box C
		%	%	%
0	control run (no fire)	0.03	0	0
1	weak wind conditions	7.4 (2.6)	0.04 (0)	0 (0)
2	moderate wind conditions	13.3	1.1	0.3
3	strong wind conditions	11.8 (56.0)	0.8 (42.4)	0 (28.3)
4	weaker fire	6.6	0.4	1.1
5	stronger fire	21.0	2.3	1.9
6	smaller fire	3.2	0.05	1.5
7	larger fire	25.7	4.0	1.6
8	line fire (perpendicular)	18.3	5.4	1.2
9	line fire (parallel)	4.6	0.5	0

Atmos. Chem. Phys. Discuss., https://doi.org/10.5194/acp-2017-1204
Manuscript under review for journal Atmos. Chem. Phys.
Discussion started: 27 April 2018

Atmospheric Chemistry and Physics Discussions

Table 3. Relative fraction of the excess of a horizontal wind velocity of 6.5 m s^{-1}, and relative fraction of a simultaneous excess of different vertical velocities of $w_1 > 0.00014$ m s^{-1}, $w_2 > 0.009$ m s^{-1}, $w_3 > 0.08$ m s^{-1}, $w_4 > 0.27$ m s^{-1}, and $w_5 > 5.1$ m s^{-1}; each within the lowest model level. The values concern to the model domain of 2 x 1.2 km shown in Fig. 9-11. Additionally, the peak values of the horizontal near-surface wind velocity and the total updraft velocity are provided.

case	description	f(v_{tres}) %	$\lvert v_{\mathrm{max,srf}} \rvert$ (m s^{-1})	f(w_1) %	f(w_2) %	f(w_3) %	f(w_4) %	f(w_5) %	$\lvert w_{\mathrm{max}} \rvert$ (m s^{-1})
0	control run (no fire)	0.008	6.7	0.007	0.007	0.006	0.004	0	5.4
1	weak wind conditions	0.09	9.9	0.09	0.09	0.08	0.08	0.02	26.6
2	moderate wind conditions	0.9	9.3	0.42	0.41	0.35	0.27	0.006	23.3
3	strong wind conditions	30.8	10.6	12.93	12.43	9.12	4.03	0.003	17.0
4	weaker fire	0.61	7.8	0.3	0.29	0.24	0.16	0	16.3
5	stronger fire	1.63	10.9	0.7	0.68	0.55	0.36	0.02	28.5
6	smaller fire	0.32	7.7	0.16	0.16	0.13	0.09	0.006	14.4
7	larger fire	2.18	10.5	0.91	0.89	0.73	0.49	0.009	25.7
8	line fire (perpendicular)	1.84	8.7	0.89	0.86	0.71	0.44	0	14.4
9	line fire (parallel)	0.34	8.0	0.15	0.15	0.12	0.09	0.0001	17.3